



**CENTRO DE INVESTIGACIÓN Y DE ESTUDIOS AVANZADOS  
DEL INSTITUTO POLITÉCNICO NACIONAL**

Unidad Mérida

**DEPARTAMENTO DE FÍSICA APLICADA**

**“La teoría variacional del estado de transición con el modelo del rotor  
impedido en *Eyringpy*”**

Tesis que presenta

**Eugenia Violeta Dzib Reyes**

para obtener el grado de

**Doctora en Ciencias**

en

**Fisicoquímica**

Director de tesis:

**Dr. José Gabriel Merino Hernández**

Mérida, Yucatán, México

Septiembre de 2022



**CENTRO DE INVESTIGACIÓN Y DE ESTUDIOS  
AVANZADOS DEL INSTITUTO POLITÉCNICO NACIONAL**

Unidad Mérida

**DEPARTAMENTO DE FÍSICA APLICADA**

**“Variational transition state theory with the hindered rotor model in  
*Eyringpy*”**

A thesis submitted by

**Eugenia Violeta Dzib Reyes**

in partial fulfillment of the requirements for the degree of

**Doctor of Science**

in

**Physical Chemistry**

Thesis advisor:

**Dr. José Gabriel Merino Hernández**

Mérida, Yucatán, México

September 2022

## **Dedication**

*To the God of my salvation*

*For thou hast possessed my reins: thou hast covered me in my mother's womb.*

*Thine eyes did see my substance, yet being imperfect; and in thy book all my members were written, which in continuance were fashioned, when as yet there was none of them.*

***Psalm 139:13,16***

## **Acknowledgments**

To God for having sought me out to allow me to know about him and his word and for having kept and sustained me until now.

To my parents for choosing me as their daughter and for all the love and support they gave me.

To my beloved husband, for being so loving and understanding during this long and sometimes complicated journey that was the doctorate.

To my mother-in-law for her advice, help, and unconditional support.

To Dr. Gabriel Merino for the guidance and academic training he gave me to carry out this project, for his patience and for encouraging me to trust in my work.

To Alan Quintal for the effort, dedication, and creativity he has put for the *Eyringpy* project.

To my friends Silvana, Charly, Raúl, and Mareny for their support and trust in me.

To Conacyt for the doctoral scholarship.

## Content

<b>LIST OF ABBREVIATIONS</b> .....	<b>II</b>
<b>ABSTRACT</b> .....	<b>1</b>
<b>RESUMEN</b> .....	<b>2</b>
<b>PREFACE</b> .....	<b>3</b>
<b>1 INTRODUCTION</b> .....	<b>6</b>
CALCULATION OF RATE CONSTANTS .....	6
VARIATIONAL TRANSITION STATE THEORY .....	15
THE HINDERED ROTOR MODEL .....	19
The model of Pitzer and Gwinn.....	23
The model of Ayala and Schlegel.....	28
REACTION SYMMETRY .....	30
PRE-REACTIVE AND PRODUCT COMPLEXES .....	32
<b>2 RESULTS</b> .....	<b>36</b>
INTRODUCTION .....	36
TECHNICALITIES .....	36
METHODS .....	39
Variational transition state theory.....	42
Hindered rotor model.....	45
Reaction symmetry .....	46
Pre-reactive and product complexes.....	47
VALIDATION .....	47
Hydrogen abstraction from formic acid by hydroxyl radical .....	48
Hydrogen abstraction from methane by hydroxyl radical .....	55
<b>3 CONCLUSIONS</b> .....	<b>59</b>
<b>APPENDIX A CONTRIBUTIONS TO THE CANONICAL PARTITION FUNCTIONS AND THERMODYNAMIC PROPERTIES.</b> .....	<b>60</b>
<b>APPENDIX B EYRINGPY USER'S MANUAL</b> .....	<b>62</b>
<b>APPENDIX C SUPPLEMENTARY INFORMATION OF CHAPTER 2</b> .....	<b>80</b>
<b>REFERENCES</b> .....	<b>82</b>

## List of abbreviations

AS	Ayala-Schlegel approximation
CT	Chuang-Truhlar approximation
CKT	Collins-Kimball theory
<i>d</i> -TST	Deformed transition state theory
DS	Dividing surface
ECK	Eckart tunneling
E2DT	Extended two-dimensional torsion
ET	Electron transfer
FR	Free rotor
GTS	Generalized transition state
GTST	Generalized transition state theory
HAT	hydrogen atom transfer
HO	Harmonic oscillator
HR	Hindered rotor
HRA	Hindered rotor for adsorbates
IRC	Intrinsic reaction coordinate
IT	Instanton theory
LCT	Large-curvature tunneling
MFG	McClurg-Flagan-Goddard approximation
MT	Marcus theory
ME	Master equation

MEP	Minimum-energy path
$\mu$ VT	Microcanonical variational transition state theory
MS-HO	Multi-structural harmonic oscillator approximation
MS-LH	Multiple-structure local harmonic approximation
MS-T(C)	Multi-structural approximation with torsional anharmonicity for a coupled torsional potential
MS-T(U)	Multi-structural approximation with torsional anharmonicity for an uncoupled torsional potential
$n$ D-HR	$n$ -dimensional hindered rotor
1D-HR	One-dimensional hindered rotor
OMT	Optimized multidimensional tunneling
RC	Pre-reactive complex
PC	Product complex
PCET	Proton-coupled electron transfer
PG	Pitzer-Gwinn approximation
PES	Potential energy surface
RFA	Reaction force analysis
RPG	Reference Pitzer-Gwinn approximation
RRHO	Rigid rotor-Harmonic oscillator approximation
RRKM	Rice-Ramsperger-Kassel-Marcus theory
SAS	Segmented Ayala-Schlegel approximation
SRPG	Segmented Reference Pitzer-Gwinn approximation

SCT	Small-curvature tunneling
TS	Transition state
TST	Transition state theory
T91	Truhlar approximation
VTST	Variational transition state theory
ZCT	Zero-curvature tunneling



---

## Abstract

*Eyringpy* is a user-friendly program for computing rate constants in the gas phase and solution based on electronic structure information. The *1.0a* version of *Eyringpy* used only transition state theory to estimate rate constants. Moreover, the reaction and activation energies are obtained by calculating from scratch the canonical partition functions under the harmonic oscillator approximation. However, the transition state theory can significantly overestimate the rate constants if the recrossing effect is significant. Also, the harmonic-oscillator approximation can lead to severe errors in describing low-frequency vibrations that are hindered rotations.

Herein, a new set of algorithms implemented in *Eyringpy* to calculate rate constants is discussed. To treat the recrossing effect, the variational transition state theory estimates rate constants based on reaction-path data (*e.g.*, electronic energies and vibrational frequencies). These data are computed for a small number of points along the reaction path. Hindered rotations are treated with the one-dimensional models of Pitzer-Gwinn and Ayala-Schlegel. Besides, in the case of bimolecular reactions pre-reactive complexes are treated by the steady-state approximation to calculate tunneling barriers. The effect of the degeneracy paths is also included. The algorithms were tested using two gas phase reactions. For both cases, near perfect accuracy was obtained compared to other programs for theoretical chemical kinetics. In the experimental case, the agreement was excellent.

---

## Resumen

*Eyringpy* es un programa amigable para calcular constantes de velocidad en fase gaseosa y en disolución con base en información de estructura electrónica. La versión 1.0a de *Eyringpy* usaba solo la teoría del estado de transición para estimar las constantes de velocidad. Además, las energías de reacción y activación se obtienen calculando desde cero las funciones de partición canónicas bajo la aproximación del oscilador armónico. Sin embargo, la teoría del estado de transición puede sobrestimar significativamente las constantes de velocidad si el efecto de recruzamiento es significativo. Además, la aproximación del oscilador armónico puede conducir a errores graves al describir las vibraciones de baja frecuencia que son rotaciones impedidas.

En este trabajo se analiza un nuevo conjunto de algoritmos implementados en *Eyringpy* para calcular constantes de velocidad. Para tratar el efecto de recruzamiento, la teoría variacional del estado de transición estima las constantes de velocidad con base en datos del camino de reacción (por ejemplo, energías electrónicas y frecuencias vibracionales). Estos datos se calculan para un pequeño número de puntos a lo largo del camino de reacción. Las rotaciones impedidas se tratan con los modelos unidimensionales de Pitzer-Gwinn y Ayala-Schlegel. Además, en el caso de reacciones bimoleculares, los complejos de pre-reactivos se tratan mediante la aproximación de estado estacionario para calcular las barreras de efecto túnel. También se incluye el efecto de la degeneración de caminos. Los algoritmos se probaron utilizando dos reacciones en fase gaseosa. En ambos casos, se obtuvo una precisión casi perfecta en comparación con otros programas de Cinética Química Teórica. En el caso experimental, la concordancia fue excelente.

**Preface**

Almost ninety years have passed since Eyring published his seminal paper “*The Activated Complex in Chemical Reactions*” in the *Journal of Chemical Physics*.<sup>1</sup> In this manuscript, he proposed the transition state theory (TST) for calculating reaction rates. For a long time, TST was viewed with skepticism. For example, in 1983, a group of prominent researchers wrote “*the validity of transition state theory has not yet been really proved and its success seems to be mysterious.*”<sup>2</sup> However, this began to change because of the advent of accurate electronic structure computations for prototype reactions of small molecules.<sup>3,4</sup> Now, TST is the basis for most calculations of rate constants.

The underlying principle of TST is that any trajectory that crosses the dividing surface (*i.e.*, the transition state, TS) from the reactant region to the product one never returns to the reactants.<sup>1</sup> Unfortunately, this is often inaccurate since real systems always have several recrossing trajectories. Therefore, the most viable option is to vary the position of the dividing surface to minimize the number of trajectories crossing it. This is the basis of variational transition state theory (VTST).<sup>4-6</sup> To calculate rate constants, obtaining the Gibbs activation energy is mandatory. The harmonic oscillator (HO) approximation is reliable to treat high-frequency vibrations.<sup>7</sup> However, it can cause large deviations for molecules with low-frequency vibrations that are hindered rotations.<sup>8-10</sup> In this case, the hindered rotor model is the option.<sup>11</sup> Another critical issue for calculating rate constant is the presence of pre-reactive complexes, mainly when tunneling is present.<sup>12-15</sup> Finally, it is essential to include the degeneracy reaction path to enhance the accuracy of the rate constants.<sup>16</sup>

A plethora of programs have been developed to compute rate constants. However, most of them have the following disadvantages: difficult installation, lack of portability and

---

maintenance, poor user-friendliness, or require the user to enter much data manually. To overcome these obstacles, *Eyringpy* was developed.

The *Eyringpy* project started in 2016 as my master's thesis topic.<sup>17</sup> During this period, I designed *Eyringpy 1.0a (pre-release version)* of the code to compute rate constants, in the gas phase and solution, *via* the TST. The Gibbs activation energy was calculated from scratch with the canonical ensemble and the HO approximation. The one-dimensional tunneling methods of Wigner<sup>18</sup> and Eckart<sup>19</sup> were also introduced. For reactions in solution, the diffusion-limit through the Collins-Kimball theory,<sup>20</sup> the study of electron transfer reactions with the Marcus theory,<sup>21,22</sup> and the effect of pH for aqueous reactions by estimating the molar fractions were included.<sup>23</sup> Subsequently, as an effort to gain an in-depth understanding of reaction mechanisms, a module to analyze primitive changes along the intrinsic reaction coordinate (IRC) was designed.<sup>24</sup> This work presents the implementation in *Eyringpy* of four methods for computing rate constants: the variational transition state theory, the hindered rotor model, the treatment of the pre-reactive and product complexes *by* the steady-state approximation, and the reaction symmetry. In addition, several new capabilities of the code are introduced, such as the rewriting of *Eyringpy* as a modular program, its binaries (for *Windows*, *Linux*, and *macOS X*), and its compatibility with other versions of *Gaussian*.

Thus, this thesis is organized into three chapters. Chapter 1 provides the basic ingredients for understanding the process of computing rate constants, the software available for this purpose, and the theoretical foundations of the new theories included in *Eyringpy* to improve the accuracy of the theoretical rate constants. Chapter 2 describes the new algorithms and functionalities of *Eyringpy*. It also discusses two representative reactions to illustrate the new capabilities of *Eyringpy*, evaluate their accuracy and validate them with

---

other software for theoretical chemical kinetics (*e.g.*, *KiSThelP*<sup>25</sup> and *TheRate*<sup>26</sup>). Chapter 3 summarizes the most important conclusions.

### 1 Introduction

#### Calculation of rate constants

The study of chemical kinetics is concerned with understanding reaction mechanisms and determining the rate constants of elementary reaction steps.<sup>27,28</sup> Traditionally, rate constants have been obtained experimentally. However, this can be a daunting task due to the numerous factors that affect reaction rates, such as the nature of reactants and solvents, concentration, temperature, pressure, light, and catalysts.<sup>27</sup> In recent decades, theoretical chemical kinetics has contributed significantly to unveiling the mechanisms of a plethora of reactions and has estimated the associated rate constants with an accuracy that rivals the best available experimental determinations,<sup>3,28</sup> particularly for conditions that are difficult or impossible to replicate in the laboratory, such as that of troposphere,<sup>29,30</sup> combustion,<sup>31-33</sup> or space conditions.<sup>34-36</sup> This resulted from dramatic advances in computational tools and capabilities and the accuracy of the theoretical methods (*i.e.*, electronic structure and chemical kinetics theories).<sup>28,31,33,37</sup> Thus, the power and usefulness of theoretical chemical kinetics, as a predictive science and to confirm the experimental observations, is evident.

How to calculate rate constants? It requires linking the microscopic quantum-mechanical properties of a molecule to the macroscopic phenomenological world. In general, it is a two-step process: The first step involves the structural and electronic characterization (geometry, vibrational frequencies, and electronic energy) of the stationary points (reactants, products, transition states, intermediaries, and reactant and/or product complexes) on the potential energy surface (PES).<sup>28,29,37</sup> This information is obtained directly from electronic structure computations performed with software such as *Gaussian*,<sup>38</sup> *Orca*,<sup>39</sup> and *ADF*.<sup>40</sup> The

second step consists of selecting a cost-effective kinetic theory.<sup>28,37</sup> The accuracy of the theoretical rate constants depends concomitantly on the quality of the level of theory used for electronic structure computations and the kinetic theory for calculating the rate constants.<sup>30</sup> Typically, the first choice is based on previous experience with similar chemical systems or by benchmarking various methods and comparing the results with experiment.<sup>41-43</sup> The second depends on the characteristics of the PES.<sup>41</sup>

Theoretical chemical kinetics has provided valuable landmarks for estimating rate constants, such as TST for pressure-independent thermal rate constants,<sup>1,44</sup> the Rice-Ramsperger-Kassel-Marcus theory (RRKM) for pressure-dependent unimolecular rate constants,<sup>45</sup> and the Marcus theory for electron transfer (ET) reactions.<sup>21,22</sup> By far, the most practical and commonly used framework is TST, proposed almost simultaneously by Eyring,<sup>1</sup> Evans and Polanyi<sup>44</sup> in 1935. TST is a statistical mechanical theory that relies on the following assumptions:

- 1) A chemical reaction proceeds *through* a minimum-energy path (MEP) on the PES connecting reactants and products.<sup>46</sup> The hypersurface separating the reactants region from the products region is the TS, *a first-order saddle point on the PES, a maximum in the reaction coordinate (s) direction and a minimum along all other coordinates* (see Figure 1.1).<sup>47</sup> The hypersurface is known as the dividing surface (DS).<sup>4</sup>
- 2) All the reaction trajectories that cross the dividing surface from the reactant zone to the products one do not cross back to the reactant zone (non-recrossing rule, see trajectory 1 in Figure 1.2). Therefore, the TS is the bottleneck of the reaction.<sup>27,30,41,46,48</sup>

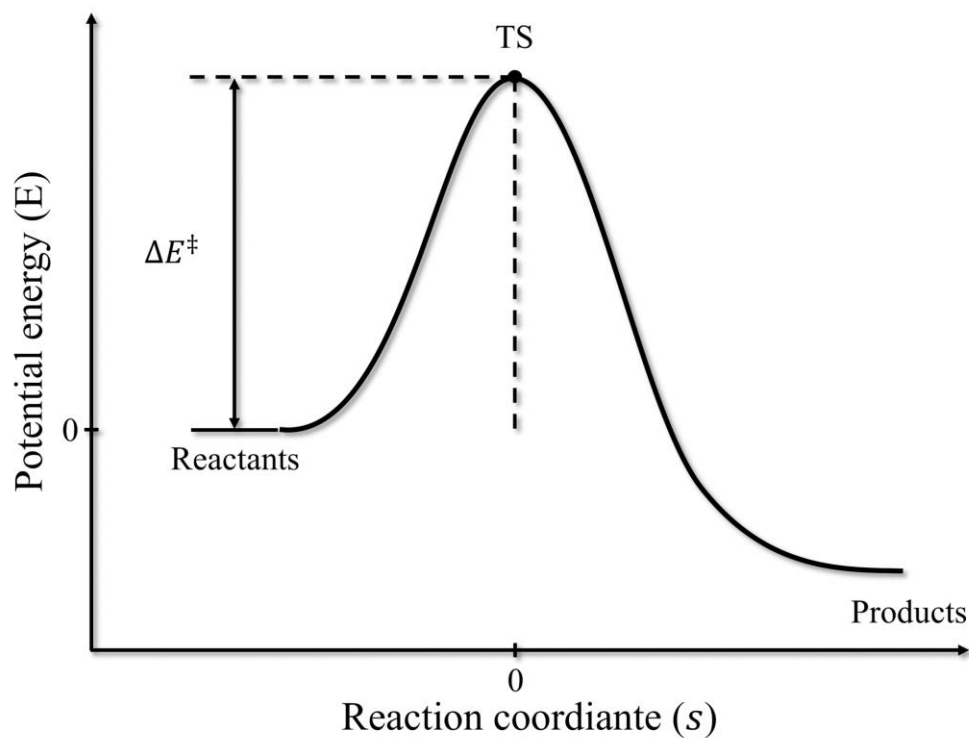


**Figure 1.1** Profile of potential energy along the reaction coordinate.  $\Delta E^\ddagger$  is the activation energy.

- 3) The reactants and TSs are assumed to have a Boltzmann distribution of energy.<sup>46-48</sup>
- 4) The motion along  $s$  can be separated from other degrees of freedom and treated classically as a free translation.<sup>46</sup>
- 5) The reactions are electronically adiabatic, *i.e.*, they take place on a single Born-Oppenheimer PES.<sup>4,48</sup>



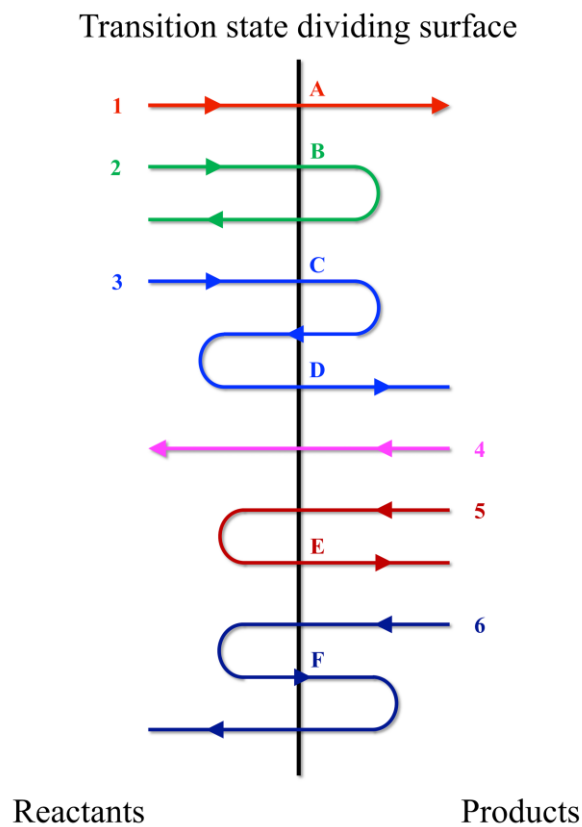


**Figure 1.2** Different ways (trajectories) in which a chemical system may go through the surface that separates the PES into the reactants region and products region. The trajectories are numbered, and the forward-crossings are lettered.

The thermodynamic form of TST rate constant is given by

$$k_{TST}(T) = \frac{k_B T}{h} e^{-\Delta G^\ddagger, 1M / RT}, \quad (1.1)$$

where  $k_B$  is the Boltzmann constant,  $h$  is the Planck constant,  $R$  is the gas constant,  $T$  is the temperature, and  $\Delta G^{\ddagger,1M}$  is the Gibbs activation energy at standard concentration ( $c^o = 1$  M) which is calculated as

$$\Delta G^{\ddagger,1M}(T) = \Delta G^{\ddagger,1atm}(T) - RT \ln [(V_m)^{-\Delta n^{\ddagger}}], \quad (1.2)$$

where  $\Delta G_{GT}^{\ddagger,1atm}$  is the Gibbs activation energy at standard pressure ( $P^o = 1$  atm),  $V_m$  is the molar volume (obtained from the ideal gas law  $PV = nRT$ ), and  $\Delta n^{\ddagger}$  is the difference in moles between TS and reactants (0 and -1 for unimolecular and bimolecular reactions, respectively).<sup>1,23,44,49</sup>

The great success of TST is because it requires only a little thermodynamic information about the reactive system. Specifically, it needs only knowledge of the PES at the saddle point and reactants.<sup>48</sup> This is practical to study a wide diversity of chemical reactions. Despite its simplicity, TST can be surprisingly accurate when the activation barrier is computed with accurate electronic structure methods,<sup>23,31,42,50,51</sup> (e.g.,  $k_{TST}$  is accurate within a factor of two for many gas phase reactions).<sup>31,51</sup> Unfortunately, TST has intrinsic limitations. One difficulty is that a real system inherently has several recrossing trajectories (see trajectories 2, 3, 5, and 6 in Figure 1.2).<sup>5,30,41</sup> Consequently, assuming non-recrossing always overestimates the rate constants! How can we minimize the recrossing? One must invoke the variational principle, *i.e.*, the position of the dividing surface along  $s$  must be variationally optimized to maximize the Gibbs activation energy in a canonical ensemble. This minimizes the rate constant and, consequently, the recrossing effect. This is the so-called

variational transition state theory (VTST).<sup>4-6,52</sup> Another obstacle for computing accurate rate constants arises from the Gibbs activation energy. From Eq. 1.1 it is deduced that an error of 1 kcal mol<sup>-1</sup> in the Gibbs activation energy leads to an error of 5.4 in  $k_{TST}$  at 298 K, an error of 2 kcal mol<sup>-1</sup> causes an error of a factor of 29.3. The Gibbs activation energy is usually obtained with the HO approximation which adequately describes most high-frequency vibrational modes.<sup>7</sup> However, it is often inaccurate for treating low-frequency modes, such as hindered rotations.<sup>8-10</sup> Hence, to improve the accuracy of the predicted Gibbs activation energy of systems with hindered rotations, it is mandatory to use the hindered rotor model.<sup>11</sup> Tunneling is a quantum phenomenon that is important for reactions involving the transference of light particles (*e.g.*, electrons and hydrogen atoms) or with narrow barriers, particularly at low temperatures.<sup>4</sup> In particular, when tunneling is significant in a bimolecular reaction leading to the formation of a pre-reactive complex that is lower in energy than the reactants, it is essential to include it in calculating the tunneling barrier.<sup>12-15</sup> Reaction symmetry is another necessary aspect to improve the accuracy of rate constants because it takes into account the path degeneracy, that is, number of different but equivalent reaction pathways that are possible.<sup>16</sup>

As mentioned, computing rate constants involves processing a large amount of data from the electronic structure output files. This process is often time-consuming and prone-to-error, even for experts. To solve this problem, theoreticians have endeavored to develop codes to perform kinetic computations automatically. A plethora of codes has been developed for this purpose (see Table 1.1). They have been written in different programming languages, such as *Python*, *Fortran*, *Java*, *Perl*, or *C++*. Most rely on TST to compute rate constants. From the available codes, three can compute VTST rate constants. To deal with one-

dimensional hindered rotations, there are three programs. As far as we know, there are no programs that include the effect of the pre-reactive complexes. However, the available kinetic programs have several types of drawbacks, such as complex installation, requiring the user to manually enter a large amount of data, a lot of external dependencies, or lack of portability.

**Table 1.1** Software available in the literature for theoretical chemical kinetics.

Software	Kinetic theory	Molecularity	Phase	Tunnel	HR theory	Language	Gui	Availability
<i>Eyringpy</i> <sup>49</sup>	TST	Uni	gas	Wigner	PG	<i>Python</i>		*
	VTST	Bi	solution	Eckart	AS			
	MT							
<i>TheRate</i> <sup>26</sup>	CKT					<i>Java</i>	*	
	TST	Uni	gas	Wigner	AS			
<i>KiSThelP</i> <sup>25</sup>	VTST	Bi		Eckart		<i>Java</i>	*	*
	RRKM							
<i>Polyrate</i> <sup>53-55</sup>	TST	Uni	gas	ZCT	CT	<i>Fortran</i>		*
	VTST	Bi	solid	SCT	AS			
	$\mu$ VT		gas-solid	LCT	RPG			
	RRKM			OMT	SRPG SAS			
<i>MultiWell</i> <sup>56</sup>	TST	Uni	gas	Eckart	1D-HR	<i>Fortran</i>		*
	$\mu$ VT	Bi						
	ME							
<i>DOIT</i> <sup>57</sup>	IT	Uni	gas					
<i>APUAMA</i> <sup>58-60</sup>		Bi	solution			<i>C++</i>	*	*
	TST	Uni	gas	Wigner				
<i>Gaussian</i> <sup>38</sup>		Bi				<i>Fortran</i>	*	*
		Uni	gas		PG			
<i>Calctherm</i> <sup>61</sup>					T91			
			gas		MFG			
<i>TAMkin</i> <sup>62</sup>					AS	<i>Python</i>		*
	TST	Uni	gas	Wigner	Schrödinger			
<i>MESMER</i> <sup>63</sup>		Bi		Eckart		<i>C++</i>		*
	ME	Uni	gas	Eckart	Schrödinger			
<i>MSTor</i> <sup>64,65</sup>						<i>Fortran</i>		*
					MS-T(U)			
					MS-T(C)			
<i>MSMC</i> <sup>66-68</sup>					MS-LH	<i>C</i>	*	*
	ME	Bi	gas	Schrödinger				
	RRKM							
<i>RMG</i> <sup>69</sup>						<i>Python</i>		*
	TST	Uni	gas	Wigner	PG			
<i>ASE</i> <sup>70</sup>						<i>Python</i>	*	*
	CKT	Bi	solution	Eckart				
<i>Q2DTor</i> <sup>71</sup>		Atom	solid		HRA			
		Mol						
<i>EStokTP</i> <sup>37</sup>						<i>Python</i>		*
	TST	Uni	gas	Eckart	MS-LH			
<i>Transitivity</i> <sup>72</sup>					E2DT	<i>Python</i>	*	*
	ME	Bi		Eckart	1D-HR			
	TST			SCT	<i>n</i> D-HR			
<i>Pilgrim</i> <sup>73</sup>						<i>Python</i>		*
	<i>d</i> -TST							
	TST	Uni	gas	SCT	E2DT			
	VTST	Bi			MS-T(C)			

\* It refers to the presence of a given feature, Mol: Molecules, Uni: Unimolecular, Bi: Bimolecular, TST: Transition state theory, VTST: Variational transition state theory,  $\mu$ VT: Microcanonical variational transition state theory, *d*-TST: Deformed transition state theory, RRKM: Rice-Ramsperger-Kassel-Marcus, ME: Master equation, MT: Marcus theory, CKT: Collins-Kimball theory, IT: Instanton theory, ZCT: Zero-curvature tunneling, SCT: Small-curvature tunneling, LCT: Large-curvature tunneling, OMT: Optimized multidimensional tunneling, Schrödinger: the hindered rotor partition function is obtained by solving the Schrödinger equation, PG: Pitzer-Gwinn approximation, T91: Truhlar approximation, MFG: McClurg-Flagan-Goddard approximation, AS: Ayala-Schlegel approximation, CT: Chuang-Truhlar approximation, RPG: Reference Pitzer-Gwinn approximation, SAS: Segmented Ayala-Schlegel approximation, SRPG: Segmented reference Pitzer-Gwinn approximation, 1D-HR: One-dimensional hindered rotor, *n*D-HR: *n*-dimensional hindered rotor, MS-T(U): Multi-structural approximation with torsional anharmonicity for an uncoupled torsional potential, MS-T(C): Multi-structural approximation with torsional anharmonicity for a coupled torsional potential, MS-LH: Multiple-structure local harmonic approximation, MS-HO: Multi-structural harmonic oscillator approximation, E2DT: Extended two-dimensional torsion, and HRA: Hindered rotor for adsorbates.

### Variational transition state theory

Transition state theory is based on the non-recrossing assumption. This states that all the trajectories originating from the reactant region cross the dividing surface of the PES only once. Consequently, all the forward-crossing trajectories end up in the product region.<sup>4-6,74,75</sup> However, a chemical system can cross the DS in several ways. For example, in Figure 1.2 six trajectories are illustrated. These can be classified as: a) Reactive trajectories (*i.e.*, trajectories connecting reactants and products)<sup>76</sup> that cross the DS directly, *e.g.*, trajectories 1 and 4, b) reactive trajectories that recross the DS, *e.g.*, trajectories 3 and 6 (trajectory 3 has two forward-crossings but only one forward-reactive one; trajectory 6 has one forward-crossing but it does not contribute to the forward-reactive flux), and c) non-reactive trajectories, *e.g.*, trajectories 2 and 5. TST considers that all trajectories contribute to the net one-way reactive flux even though only 1 and 3 contribute to the net one-way reactive flux.<sup>5</sup> Consequently, TST overestimates the rate constant. This worsens as the activation barrier lowers and the temperature increases.<sup>41,77,78</sup>

The failure of the TST is due to the recrossing effect. TST locates the DS at the first-order saddle point of the PES (*i.e.*, at the TS, Figure 1.1).<sup>5</sup> The ideal position of the DS would be one at which all the trajectories from the reactant region cross the DS and never return. However, for real PESs it is impossible to remove all the recrossing. Hence, VTST variationally optimizes the position of the dividing surface along the MEP to maximize the generalized Gibbs activation energy  $\Delta G_{GTST}^{1M}$  (*i.e.*, the ZPE and entropic effects are included, see Figure 1.3).<sup>4,5,75</sup> The resulting dividing surface is a generalized transition state (GTS).<sup>5</sup> VTST is equivalent to minimize the generalized TST rate constant  $k_{GTST}$ .

---

$$\Delta G_{VTST}^{1M}(T) = \max_s \Delta G_{GTST}^{1M}(T, s) \quad (1.3)$$

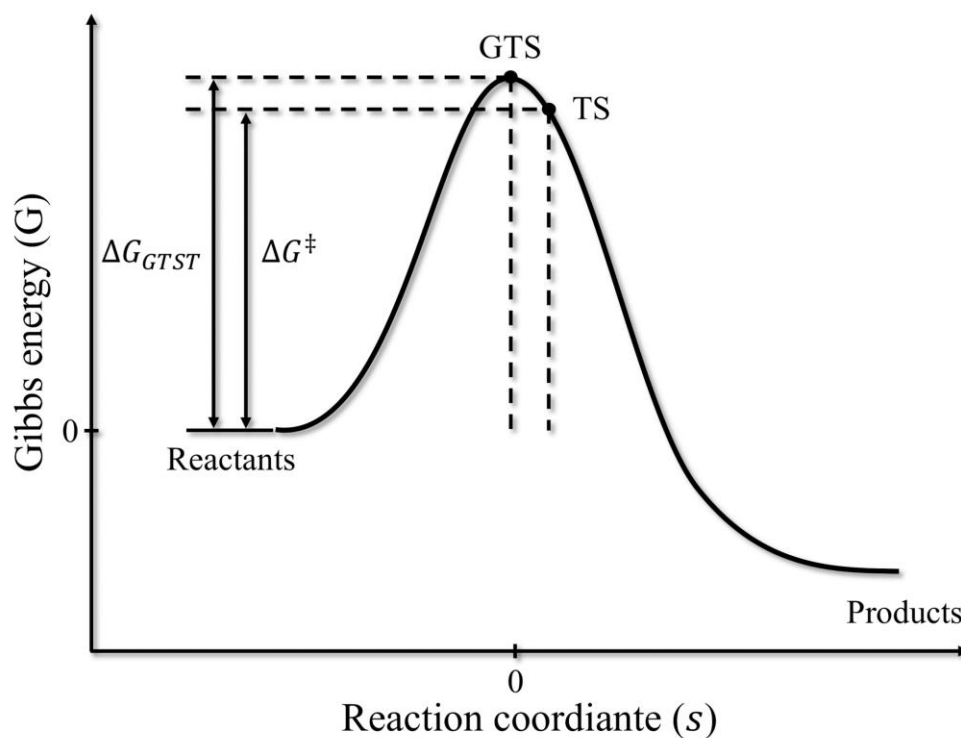


**Figure 1.3** Profile of Gibbs energy along the reaction coordinate.  $\Delta G^\ddagger$  is the Gibbs activation energy, and  $\Delta G_{GTST}$  is the generalized Gibbs activation energy.

For a canonical ensemble, the VTST rate constant is computed by

$$k_{VTST}(T) = \min_s k_{GTST}(T, s) = k_{GTST}[T, s_{VTST}^*(T)], \quad (1.4)$$



where  $s_{VTST}^*$  is the position of the dividing surface that minimizes the GTST rate constant at temperature  $T$ .<sup>4,5,52</sup> Note that if the GTS is located at the saddle point, Eq. 1.4 converges to  $k_{TST}$ .<sup>26</sup> The reaction coordinate  $s$  is the distance along the MEP in iso-inertial coordinates (*e.g.*, mass-weighted Cartesians or mass-scaled Cartesians).<sup>4</sup> The MEP is the union of the paths of steepest descent from the saddle point toward reactants and products. Its origin is the saddle point ( $s = 0$ ), it is positive on the product side ( $s > 0$ ), and negative on the reactant side ( $s < 0$ ).<sup>4,5</sup>

The thermodynamic form of the GTST rate constant is given by<sup>4</sup>

$$k_{GTST}(T, s) = \frac{k_B T}{h} e^{-\Delta G_{GTST}^{1M}(T, s)/RT}, \quad (1.5)$$

where  $\Delta G_{GTST}^{1M}$  is obtained from the equilibrium constant in terms of concentrations,  $K_{c,GTST}$ , expressed as

$$K_{c,GTST} = K_{p,GTST} (V_m)^{-\Delta n_{GTST}}, \quad (1.6)$$

$$e^{-\Delta G_{GTST}^{1M}(T, s)/RT} = e^{-\Delta G_{GTST}^{1atm}(T, s)/RT} (V_m)^{-\Delta n_{GTST}}, \quad (1.7)$$

where,  $K_{p,GTST}$  is the equilibrium constant in terms of partial pressures,  $\Delta G_{GTST}^{1atm}$  is the generalized Gibbs activation energy at standard pressure ( $P^o = 1$  atm),  $V_m$  is the molar volume (obtained from the ideal gas law  $PV = nRT$ ), and  $\Delta n_{GTST}$  is the difference in moles between the GTS and the reactants (0 and -1 for unimolecular and bimolecular reactions,

---

respectively). Therefore, the generalized Gibbs activation energy at standard concentration ( $c^o = 1 \text{ M}$ ), is obtained as<sup>23</sup>

$$\Delta G_{GTST}^{1M}(T, s) = \Delta G_{GTST}^{1atm}(T, s) - RT \ln[(V_m)^{-\Delta n_{GTST}}], \quad (1.8)$$

$$\Delta G_{GTST}^{1atm}(T, s) = \left[ G_{GTS}(T, s) + E_{GTS}(s) \right] - \sum_{i=1}^2 \left[ G_{R_i}(T) + E_{R_i}(s) \right], \quad (1.9)$$

where  $G_{GTS}$  and  $E_{GTS}$  are the Gibbs energy and the electronic energy of the GTS, respectively; and  $G_{R_i}$  and  $E_{R_i}$  are the Gibbs energy and the electronic energy of the  $i^{th}$  reactant.

## The hindered rotor model

Although the concept of hindered rotation (also called restricted rotation, internal rotation, or torsion) is quite old,<sup>79</sup> it lacks a precise definition. In a broad sense, IUPAC defines hindered rotation as: “*the inhibition of rotation of groups about a bond due to the presence of a sufficiently large rotational barrier to make the phenomenon observable on the time scale of the experiment.*”<sup>80</sup> In quantum chemistry, hindered rotation is a type of low-frequency vibrational mode for which the HO approximation is wild inaccurate.<sup>81,82</sup> During a hindered rotation, one molecular fragment (called “the top or hindered rotor, HR”) rotates relative to another (called “the frame”) around a bond (Figure 1.4).<sup>8,81,83</sup>

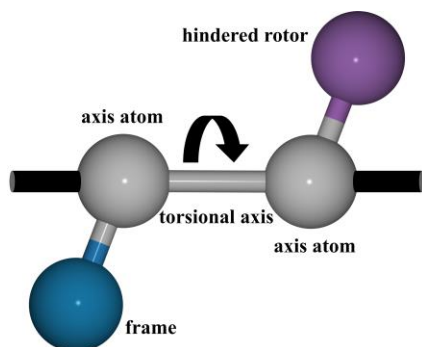


**Figure 1.4** General definition of a hindered rotor.

There are two types of hindered rotors. A symmetric hindered rotor is one whose moments of inertia perpendicular to the torsional axis are equal. This results from symmetrically placing identical atoms (*e.g.*,  $-\text{CH}_3$ , the prototype hindered rotor). Specifically, this is an identically symmetric hindered rotor. There are also cases when a hindered rotor is formed by several different atoms placed in such a way that the moments of inertia are equal, so they are called accidentally symmetric hindered rotors.<sup>84</sup> In contrast, unsymmetric

hindered rotors are divided into balanced, small off-balanced, and large off-balanced hindered rotors. Balanced HRs have their center of gravity at their torsional axis, such balance being accidental or due to a two-fold symmetry axis (*e.g.*, the phenyl substituent). Small off-balanced HRs cause a minor change in the overall (*i.e.*, external) moments of inertia when rotating (*e.g.*, -OH, -NH<sub>2</sub>, and -CH<sub>2</sub>D).<sup>84</sup> Importantly, ample off-balanced HRs while rotating cause significant changes in the overall moments of inertia that are too difficult to ignore (*e.g.*, -CH<sub>2</sub>Cl, -CHBr<sub>2</sub>, and -CHO) (see Figure 1.5).<sup>85</sup>

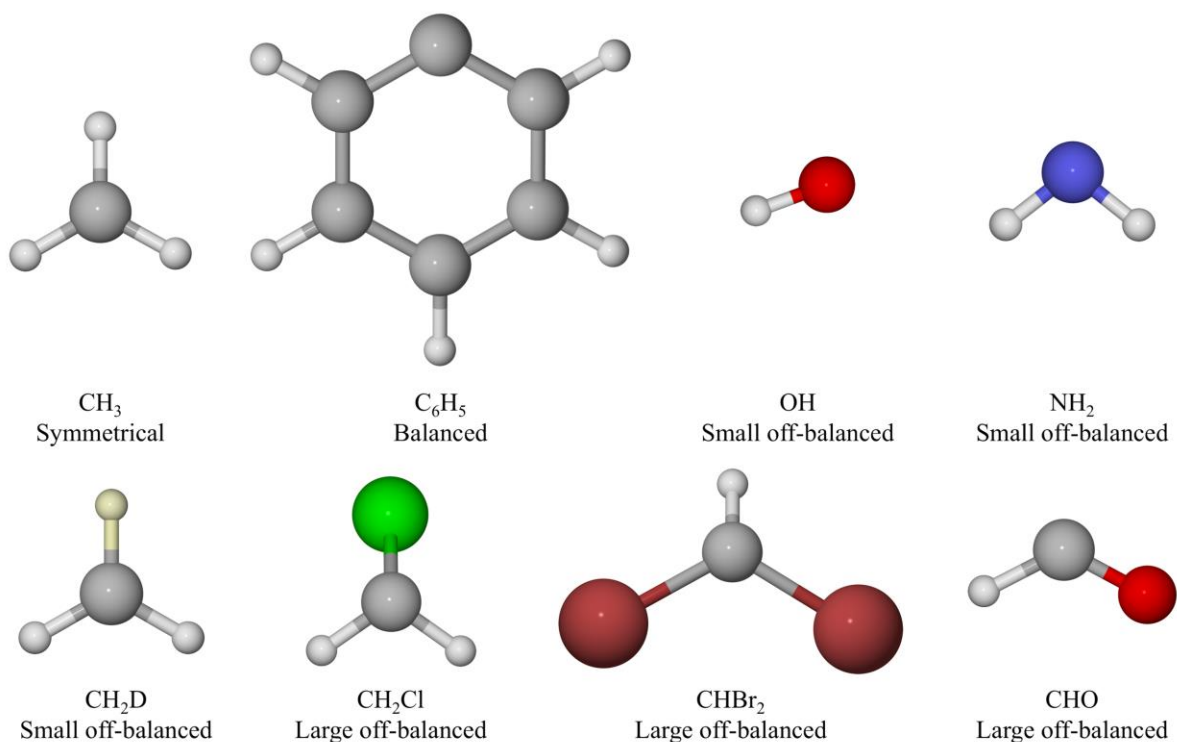


**Figure 1.5** Examples of the different types of hindered rotors (symmetric and unsymmetric).

The thermodynamic properties are computed after a structural and electronic characterization (geometry, electronic energy, and vibrational frequencies) of the chemical system(s).<sup>47,86-88</sup> The partition function is the bridge between the microscopic quantum-mechanical properties of a molecule and its macroscopic thermodynamic properties, defined in the canonical ensemble as

$$q = \sum_j e^{-E_j/k_B T}, \quad (1.10)$$

where  $E_j$  is the energy of the  $j^{\text{th}}$  state.<sup>89</sup> Strictly speaking, obtaining the total energy of a system involves the exact solution of the Schrödinger equation. However, the computations are simplified by invoking the Born-Oppenheimer, ideal gas, and rigid-rotor harmonic-oscillator (RRHO) approximations. As a result, the translational, rotational, vibrational, and electronic degrees of freedom are decoupled, and the partition function is computed as<sup>47,87</sup>

$$q = q_{\text{trans}} q_{\text{rot}} q_{\text{vib}} q_{\text{elec}}, \quad (1.11)$$

The translational, rotational, and electronic partition functions can be computed by standard methods (*e.g.*, the rigid rotor) (Table A1, Appendix A).<sup>49,86,89</sup> In contrast, vibrations are more complicated to deal with. In general, the HO approximation adequately describes most high-frequency vibrational modes<sup>53</sup> but is often inaccurate for treating low-frequency modes, such as hindered rotations.<sup>8-10</sup> In particular, at low temperatures or high barriers (*i.e.*,  $V_0 \gg k_B T$ ), hindered rotations can be treated as harmonic oscillators. At high temperatures,

---

or for low barriers (*i.e.*,  $V_0 \ll k_B T$ ), the free rotor (FR) is a better approximation.<sup>67,90,91</sup> Therefore, it is mandatory to use a proper model to improve the accuracy of the predicted thermodynamic properties for systems with hindered rotations.

The simplest way to compute the vibrational partition function of a chemical system with torsions is to assume that the normal modes are decoupled. The non-torsional modes are treated using the HO approximation while the torsions are considered under the one-dimensional hindered rotor (1D-HR) approximation. As a result, the vibrational partition function can be written as

$$q_{vib}^{HO-HR} = q_{HO} q_{HR}, \quad (1.12)$$

$$q_{HO} = \prod_{i=1}^F \frac{e^{-h\nu_i/2k_B T}}{1 - e^{-h\nu_i/k_B T}}, \quad (1.13)$$

where  $q_{HO}$  and  $q_{HR}$  are the partition functions of the quantum harmonic oscillator and hindered rotor, respectively;  $F$  is the number of non-torsional modes, and  $\nu_i$  is the vibrational frequency of the  $i^{th}$  non-torsional mode.<sup>81,89</sup>

Consequently, the total partition function for a molecule with torsions is calculated as

$$q = q_{trans} q_{rot} q_{elec} q_{vib}^{HO-HR}. \quad (1.14)$$

**The model of Pitzer and Gwinn**

One of the most widely used methods for dealing with torsions was first derived by Pitzer and Gwinn<sup>84</sup> in the 1940s, who solved the Schrödinger equation numerically for the one-dimensional hindered rotor (1D-HR)

$$-\frac{\hbar^2}{2I_r} \frac{d^2\psi_{HR}}{d\varphi^2} + V_\tau\psi_{HR} = E_{HR}\psi_{HR}, \quad (1.15)$$

where  $\psi_{HR}$  is the wave function of the hindered rotor,  $\varphi$  is the torsional angle,  $E_{HR}$  is the energy,  $I_r$  is the reduced moment of inertia,  $\hbar$  is the Dirac constant, and  $V_\tau$  is the torsional potential given by

$$V_\tau = \frac{V_0}{2} (1 - \cos M\varphi), \quad (1.16)$$

in this case,  $V_0$  is the torsional barrier, and  $M$  is total number of minima along the torsional coordinate (in the range  $0-2\pi$ ). It is important to highlight that for symmetrical HRs  $M$  is equal to the torsional symmetry number  $\sigma_\tau$ . Eq. 1.15 can be transformed into the Mathieu equation<sup>92,93</sup> and solved to obtain the energy eigenvalues, from which the partition function and thermodynamic properties are evaluated. Pitzer and Gwinn tabulated the entropy, Gibbs energy, and heat capacity for many parameters accurately.<sup>84</sup> These tables have been used for many years to benchmark other HR schemes.<sup>8,94,95</sup>

---

In addition, Pitzer and Gwinn suggested an analytical expression (called the PG model) of the hindered rotor partition function by correcting the classical partition function,  $q_{class}$ , with the ratio of the quantum and classical harmonic oscillator partition functions,  $q_{HO}$  and  $q_{CHO}$ , respectively.

$$q_{HR}^{PG} = q_{class} \left( \frac{q_{HO}}{q_{CHO}} \right), \quad (1.17)$$

$$q_{HO} = \frac{e^{-h\nu_\tau/2k_B T}}{1 - e^{-h\nu_\tau/k_B T}} \quad (1.18)$$

$$q_{CHO} = \frac{k_B T}{h\nu_\tau}, \quad (1.19)$$

$$q_{class} = \frac{(2\pi k_B T)^{1/2}}{h} \int_0^{2\pi/M} I_r^{1/2} e^{-(V_0/2RT)(1-\cos M\phi)} d\phi, \quad (1.20)$$

where  $\nu_\tau$  is the torsional frequency.<sup>84</sup> When a symmetric HR (*e.g.*, the methyl group) rotates its  $I_r$  remains constant,<sup>61</sup> which leads to

$$q_{class} = q_{FR} e^{-V_0/2RT} I_0(V_0/2RT), \quad (1.21)$$

$$q_{FR} = \frac{(8\pi^3 I_r k_B T)^{1/2}}{Mh}, \quad (1.22)$$



in this case,  $q_{FR}$  is the free rotor partition function,  $I_0$  is the modified Bessel function of the first type of zeroth-order.<sup>8</sup>  $I_r$  can be obtained by the exact method of Pitzer and Gwinn in the case of molecules with a single symmetric HR.<sup>84</sup> The PG model is accurate for systems with one torsion and a potential as in Eq. 1.16, but it also works well for systems with widely separated HRs. Therefore, the PG model can be extended to multiple rotors.

$$q_{HR}^{PG} = \prod_{i=1}^T q_{class_i} \left( \frac{q_{HO_i}}{q_{CHO_i}} \right), \quad (1.23)$$

where  $T$  is the number of torsional modes.

To compute the HR thermodynamic properties (internal energy, enthalpy, entropy, and Gibbs energy) through the PG model, the Eq. 1.23 must be substituted into the well-known equations found in the literature (Table A2, Appendix A).<sup>89,96,97</sup> The different HR contributions to the thermodynamic properties using the PG model are listed in Tables 1.2-1.3. The thermodynamic properties of the hindered rotor are computed by

$$U_{HR}^{PG} = U_{HO}^{PG} - U_{CHO}^{PG} + U_{class}^{PG} \quad (1.24)$$

$$H_{HR}^{PG} = H_{HO}^{PG} - H_{CHO}^{PG} + H_{class}^{PG} \quad (1.25)$$

$$S_{HR}^{PG} = S_{HO}^{PG} - S_{CHO}^{PG} + S_{class}^{PG} \quad (1.26)$$

$$G_{HR}^{PG} = G_{HO}^{PG} + G_{CHO}^{PG} + G_{class}^{PG} \quad (1.27)$$

**Table 1.2** Contributions to internal energy and entropy, per mole of substance.

	Internal energy	Entropy
<b>Free rotor</b>	$U_{FR}^{PG} = \sum_{i=1}^T \frac{1}{2} RT$	$S_{FR}^{PG} = \sum_{i=1}^T \left( \frac{1}{2} + \ln q_{FRi} \right) R$
<b>Classical harmonic oscillator</b>	$U_{CHO}^{PG} = \sum_{i=1}^T RT$	$S_{CHO}^{PG} = \sum_{i=1}^T (1 + \ln q_{CHOi})$
<b>Quantum harmonic oscillator</b>	$U_{HO}^{PG} = \sum_{i=1}^T \left( \frac{h\nu_{\tau_i}}{k_B} \right) \left( \frac{1}{2} + \frac{1}{e^{h\nu_{\tau_i}/k_B T} - 1} \right) R$	$S_{HO}^{PG} = \sum_{i=1}^T \left[ \frac{h\nu_{\tau_i}/k_B T}{e^{h\nu_{\tau_i}/k_B T} - 1} - \ln(1 - e^{-h\nu_{\tau_i}/k_B T}) \right] R$
<b>Classical</b>	$U_{class}^{PG} = \sum_{i=1}^T \frac{1}{2} \left[ 1 + y - y \frac{I_1(y/2)}{I_0(y/2)} \right] RT$	$S_{class}^{PG} = \sum_{i=1}^T \left[ \frac{1}{2} \left[ 1 - y \frac{I_1(y/2)}{I_0(y/2)} \right] + \ln[q_{FRi} I_0(y/2)] \right] R$

$y = V_0/RT$ .  $I_0$  is the modified Bessel function of the first kind of zeroth-order.  $I_1$  is the modified Bessel function of the first kind of first order.

**Table 1.3** Contributions to enthalpy and Gibbs energy, per mole of substance.

	Enthalpy	Gibbs energy
<b>Free rotor</b>	$H_{FR}^{PG} = \sum_{i=1}^T \frac{1}{2} RT$	$G_{FR}^{PG} = - \sum_{i=1}^T RT \ln q_{FRi}$
<b>Classical harmonic oscillator</b>	$H_{CHO}^{PG} = \sum_{i=1}^T RT$	$G_{CHO}^{PG} = \sum_{i=1}^T RT \ln q_{CHOi}$
<b>Quantum harmonic oscillator</b>	$H_{HO}^{PG} = \sum_{i=1}^T \left( \frac{h\nu_{\tau_i}}{k_B} \right) \left( \frac{1}{2} + \frac{1}{e^{h\nu_{\tau_i}/k_B T} - 1} \right) R$	$G_{HO}^{PG} = \sum_{i=1}^T \left[ \frac{h\nu_{\tau_i}}{2k_B T} + \ln(1 - e^{-h\nu_{\tau_i}/k_B T}) \right] RT$
<b>Classical</b>	$H_{class}^{PG} = \sum_{i=1}^T \frac{1}{2} \left[ 1 + y - y \frac{I_1(y/2)}{I_0(y/2)} \right] RT$	$G_{class}^{PG} = \sum_{i=1}^T RT [(y/2) - \ln[q_{FR} I_0(y/2)]]$

$y = V_0/RT$ .  $I_0$  is the modified Bessel function of the first kind of zeroth-order.  $I_1$  is the modified Bessel function of the first kind of first order.

### The model of Ayala and Schlegel

The method proposed by Ayala and Schlegel (AS) adjusts the PG scheme (Eq. 1.17) by a multiplicative factor to achieve better results for small torsional barriers and high temperatures by a polynomial factor (Eq. 1.28).

$$q_{HR}^{AS} = \sum_{i=1}^T q_{classi} \left( \frac{q_{HOi}}{q_{CHOi}} \right) \left( \frac{1 + P_2 e^{-V_0/2RT}}{1 + P_1 e^{-V_0/2RT}} \right), \quad (1.28)$$

where  $P_1$  and  $P_2$  are fifth-order polynomial functions of  $x = 1/q_{FR}$  and  $y = V_0/RT$  (Table A3, Appendix A), and the torsional barrier is

$$V_0 = \frac{8\pi^2 v_\tau^2 I_r N_A}{M^2}, \quad (1.29)$$

where  $N_A$  is the Avogadro constant.<sup>8</sup>

The thermodynamic properties using the AS model are calculated in the same way as in the PG one. The different contributions to the thermodynamic properties using the AS model are listed in Table 1.4.

$$U_{HR}^{AS} = U_{HO}^{AS} - U_{CHO}^{AS} + U_{class}^{AS} \quad (1.30)$$

$$H_{HR}^{AS} = H_{HO}^{AS} - H_{CHO}^{AS} + H_{class}^{AS} \quad (1.31)$$

$$S_{HR}^{AS} = S_{HO}^{AS} - S_{CHO}^{AS} + S_{class}^{AS} \quad (1.32)$$

$$G_{HR}^{AS} = G_{HO}^{AS} + G_{CHO}^{AS} + G_{class}^{AS} \quad (1.33)$$

**Table 1.4** Internal energy, entropy, enthalpy, and Gibbs energy according to the hindered rotor model of Ayala and Schlegel, per mole of substance.

**Internal  
energy**

$$U_{HR}^{AS} = U_{HR}^{PG} + \sum_{i=1}^T \left[ \frac{(y/2)P_2 + P_4}{1 + P_2 e^{-y/2}} - \frac{(y/2)P_1 + P_3}{1 + P_1 e^{-y/2}} \right] e^{-y/2} RT$$

**Entropy**

$$S_{HR}^{AS} = S_{HR}^{PG} + \sum_{i=1}^T \left[ \left[ \frac{(y/2)P_2 + P_4}{1 + P_2 e^{-y/2}} - \frac{(y/2)P_1 + P_3}{1 + P_1 e^{-y/2}} \right] e^{-y/2} + \ln \left( \frac{1 + P_2 e^{-y/2}}{1 + P_1 e^{-y/2}} \right) \right] R$$

**Enthalpy**

$$H_{HR}^{AS} = H_{HR}^{PG} + \sum_{i=1}^T \left[ \frac{(y/2)P_2 + P_4}{1 + P_2 e^{-y/2}} - \frac{(y/2)P_1 + P_3}{1 + P_1 e^{-y/2}} \right] e^{-y/2} RT$$

**Gibbs energy**

$$G_{HR}^{AS} = G_{HR}^{PG} - \sum_{i=1}^T RT \left[ \ln \left( \frac{1 + P_2 e^{-y/2}}{1 + P_1 e^{-y/2}} \right) \right]$$

$P_3 = T(\partial P_1 / \partial T)$  and  $P_4 = T(\partial P_2 / \partial T)$  are fifth order polynomial functions (Table A3, Appendix A).

### Reaction symmetry

The reaction symmetry number  $\sigma_{Rx}$  represents the number of different but equivalent reaction pathways that are possible. It is also known as the reaction path degeneracy. In general, it is given by the product of the symmetry numbers of the reactants ( $\sigma_i^R$ ) divided by the symmetry number of the TS ( $\sigma^\ddagger$ ) as

$$\sigma_{Rx} = \frac{\prod_{i=1}^n \sigma_i^R}{\sigma^\ddagger}, \quad (1.34)$$

where  $n$  is the number of reactants.<sup>98</sup>

In TST, the rotational symmetry number of the TS is constant. However, in VTST the rotational symmetry number of the GTS varies along the reaction coordinate. In this case, the reaction path degeneracy is obtained as

$$\sigma_{Rx}(s) = \frac{\prod_{i=1}^n \sigma_i^R}{\sigma_{GTS}(s)}, \quad (1.35)$$

where  $\sigma_{GTS}(s)$  is the rotational symmetry number of the GTS.<sup>26</sup>

This method is valid for most reactions. Nevertheless, to calculate  $\sigma_{Rx}$  for reactions where chiral isomers, conformers or HRs are present, it is important to consider not just the rotational symmetry numbers. For this purpose, the approach of Fernández-Ramos *et al.* is recommended.<sup>16</sup>

To compute rate constants including the reaction path degeneracy, the rotational symmetry numbers must be factored out from the partition functions (Table A1, Appendix A), and thus

$$k_{TST}(T) = \sigma_{Rx} \frac{k_B T}{h} e^{-\Delta G^{\ddagger,1M}/RT}, \quad (1.36)$$

and

$$k_{GTST}(T, s) = \sigma_{Rx}(s) \frac{k_B T}{h} e^{-\Delta G_{GTST}^{1M}(T, s)/RT}. \quad (1.37)$$

### Pre-reactive and product complexes

What are pre-reactive complexes? IUPAC defines pre-reactive complexes as “*Weakly bound complexes with a potential minimum that precedes the activation barrier along the reaction path. In contrast with the van der Waals complexes, which fall apart reversibly into their constituents, the pre-reactive complexes may undergo a vigorous reaction to form different products.*”<sup>99</sup> Consideration of the pre-reactive complex is crucial accurately estimate the rate constants of bimolecular reactions when the tunneling effect is significant, as in the case of hydrogen abstraction reactions.<sup>12-15</sup> To calculate the rate constants in these cases, the method proposed by Alvarez-Idaboy *et al.*<sup>12</sup> is one of the best options. This approach is based on the assumption that a bimolecular reaction proceeds following a two-step mechanism, in which the initial step involves the formation of a pre-reactive complex (RC) that is in equilibrium with the reactants (R), and the second step is the irreversible formation of the products (P). In addition, several reactions can lead to the formation of a product complex (PC) (see Figure 1.6):



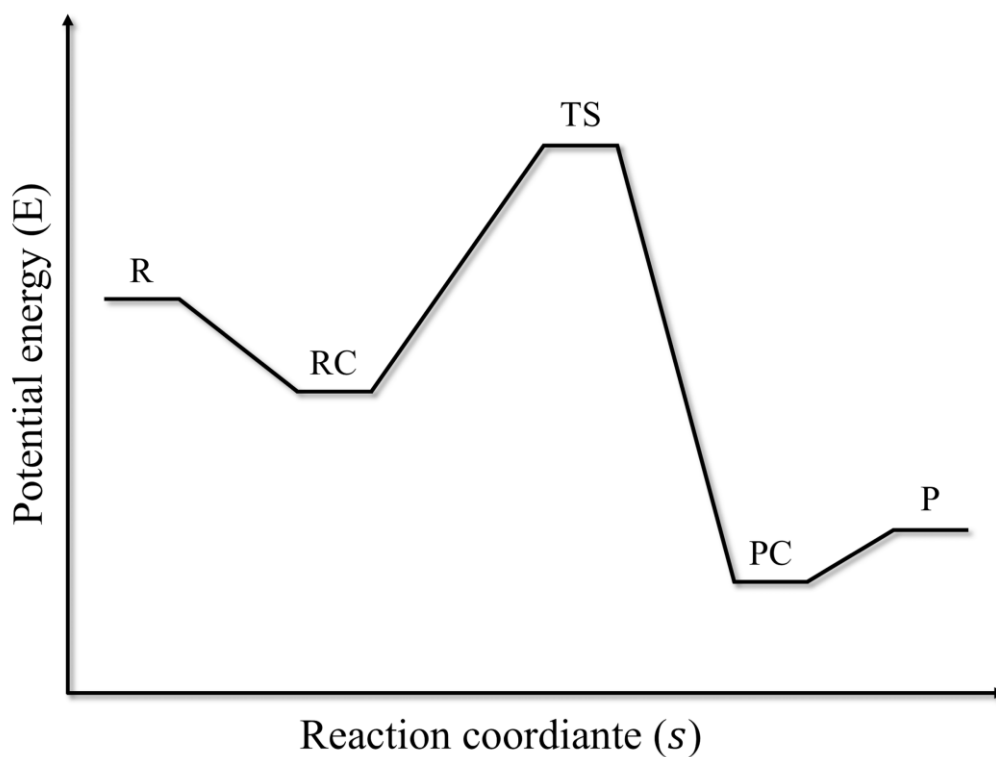
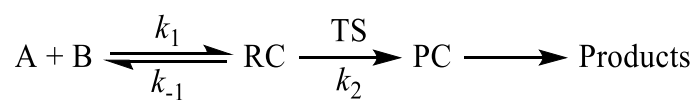


**Figure 1.6** Profile of potential energy along the reaction coordinate for a reaction leading to the formation of pre-reactive and product complexes.



In this equation,  $k_1$  and  $k_{-1}$  are the forward and reverse rate constants, respectively, for the first step, and  $k_2$  is the forward rate constant corresponding to the second step. Applying the steady-state approximation to this mechanism leads to the following rate constant

$$k = \frac{k_1 k_2}{k_{-1}} = K_1 k_2, \quad (1.38)$$

where the equilibrium constant between the reactants and the pre-reactive complex,  $K_1$ , and the rate constant of the second step,  $k_2$ , are calculated as follow

$$K_1 = e^{-\Delta G_1/RT}, \quad (1.39)$$

$$k_2^{TST} = \frac{k_B T}{h} e^{-\Delta G_2^\ddagger/RT}, \quad (1.40)$$

where  $\Delta G_1 = G_{RC} - G_R$  is the Gibbs stabilization energy of the pre-reactive complex and  $\Delta G_2^\ddagger = G_{TS} - G_{RC}$  is the Gibbs activation energy of the second step.<sup>12</sup> In VTST, the Gibbs stabilization energy of the pre-reactive complex is  $\Delta G_2^{GT}(T, s) = G_{GT}(T, s) - G_{RC}(T)$  and the rate constant of the second step is calculated as<sup>100</sup>

$$k_2^{VTST}(T, s) = \frac{k_B T}{h} e^{-\Delta G_2^{GT}(T, s)/RT}, \quad (1.41)$$

In both cases, the Gibbs energy of the pre-reactive complex,  $G_{RC}$ , is canceled out and the TST rate constants are estimated with Eq. 1.36. VTST rate constants are calculated with Eqs. 1.4 and 1.37.

---

Consequently,  $k$  does not include the RC explicitly. Nevertheless, when the Eckart tunneling correction,  $\kappa_{Eck}$ , is applied,<sup>19</sup> the pre-reactive and product complexes are considered in the values of the activation enthalpies at 0 K for the forward and reverse reactions,  $\Delta H_f^{\ddagger,0K}$  and  $\Delta H_r^{\ddagger,0K}$ , respectively.<sup>14,15</sup>

## 2 Results

### Introduction

This Chapter describes the methods and functionalities that have been added to *Eyringpy* after its *1.0a* version:<sup>17</sup> The variational transition state theory, the hindered rotor model, the treatment of the pre-reactive and product complexes, and the reaction symmetry. It also includes the validation of the implemented algorithms. *Eyringpy 1.0a* was based on TST<sup>1,44</sup> for computing rate constants in the gas phase and solution. In that version, the reaction and activation barriers are calculated with the canonical ensemble considering that the species participating in the reaction behave as ideal gases and obey the RRHO approximation.<sup>89,96</sup> Moreover, the effects of tunneling,<sup>18,19</sup> diffusion,<sup>20</sup> electron transfer,<sup>21,22</sup> and pH are included.<sup>23</sup> That version of the code parsed the input parameters from electronic structure computations performed only with *Gaussian 09*, Rev. A.02.<sup>101</sup> *Eyringpy 1.0a* was written in *Python 2.6* as a non-modular, open-source, and *Linux*- and *macOS X*-compatible code.

### Technicalities

Substantial advances have been made to *Eyringpy*. A summary of the changes with respect to the *1.0a* version is given in Table 2.1. Now, let us describe the main new features in *Eyringpy*:

**Table 2.1** Comparison of the features of the most recent release of *Eyringpy* with those of its *1.0a* version.

	<i>Eyringpy 1.0a</i>	<i>Eyringpy</i> latest release
<b>Kinetic theory</b>	TST, MT, CKT	TST, VTST, MT, CKT
<b>Tunnel</b>	Wigner, Eckart	Wigner, Eckart
<b>pH effect</b>	*	*
<b>HR theory</b>		PG, AS
<b>Reactant and Product complex</b>		*
<b>Reaction symmetry</b>		*
<b>Gibbs activation energy</b>	1 atm	1 atm, 1 M
<b>Phase and molecularity</b>	Uni: Gas	Uni: Gas, solution
	Bi: Gas, solution	Bi: Gas, solution
<b>Temperature</b>	298 K: Solution	All: Gas, solution
	All: Gas	
<b>Python version</b>	2.6	3.9
<b>Modular</b>		*
<b>Compatibility</b>	<i>Linux, macOS X</i>	<i>Windows, Linux, macOS X</i>
	64 bits	32 bits, 64 bits
<b>Binaries</b>		*
<b>Electronic structure software</b>	<i>Gaussian 09: Rev. A.02</i>	<i>Gaussian 09: Rev. A.02, D.01</i> <i>Gaussian 16: Rev. B.01</i>
<b>Electronic structure theory</b>	DFT, MP2	DFT, MP2, CCSD(T)
<b>Electronic structure methods database</b>		*
<b>Viscosity database</b>		*

- 1) Programming paradigm: One of the most significant changes in *Eyringpy*'s design philosophy is that the code was rewritten from scratch with a modular structure. This makes it reusable and easy to maintain, test, and debug. So, *Eyringpy* modules can be easily modified or extended with minimal changes to other modules.
- 2) Computing time: *Eyringpy* functions were redesigned to provide multiple outputs, significantly reducing the time needed to perform a task (*e.g.*, for iterations over a large amount of data).
- 3) Programming language upgrade: *Eyringpy* has been ported to *Python3* for faster and more readable code.
- 4) Compatibility and portability: The binaries (for 32 and 64 bits) of *Eyringpy* (for *Windows*, *Linux*, and *macOS X*) have been built using *PyInstaller*. This module bundles *Python* programs and all their dependencies into a single package. Hence, *Eyringpy* is offered as an out-of-the-box program, *i.e.*, the user can execute it without installing the *Python* interpreter or any modules or third-party libraries. However, in the case of *Linux*, it is necessary to install the *glibc* library.
- 5) *Gaussian* output files: *Eyringpy* extracts the input data needed to compute rate constants from the output files of electronic structure computations performed with *Gaussian*. The current version was adapted to handle the output file formats of *Gaussian 09* Rev. D.01<sup>102</sup> and *Gaussian 16* Rev. B.01.<sup>38</sup> Particularly, the \*.log extension (typical of the *Windows* version of *Gaussian*) of these files is now available. Furthermore, a tool was designed to check if all the electronic structure

computations are at the same level or if they end normally. For this purpose, it was necessary to build a database of levels.

- 6) *Gaussian* input files: A module (called *writeInp*) was developed to create input files for *Gaussian* computations. The available jobs are single-point energy, geometry optimization, frequency analysis, IRC, PES scan, and volume.
- 7) Electronic structure methods: A code was generated to analyze the electronic structure data obtained at the CCSD(T) level to improve the quality of reaction and activation barriers.
- 8) Activation energies: Gibbs activation energies are calculated also at standard state 1M.
- 9) Rate constants in solution: A viscosity database of liquids<sup>103</sup> was added to *Eyringpy* to estimate rate constants of reactions in solution at different temperatures. The option to study unimolecular reactions in solution was also included.
- 10) Bug fixing and warnings: The code was modified to fix several bugs arising from typos in the *Gaussian* output files. A series of warnings are displayed to alert the user.

### Methods

The flowchart for computing rate constants is depicted in Figure 2.1 First, it is mandatory to create an input file (see the user's manual in Appendix B for more details). Then, *Eyringpy* extracts data from the electronic structure output files of the species involved

in the reaction. Finally, the program computes the rate constants according to the desired methods. The new implemented methods will now be described in detail.



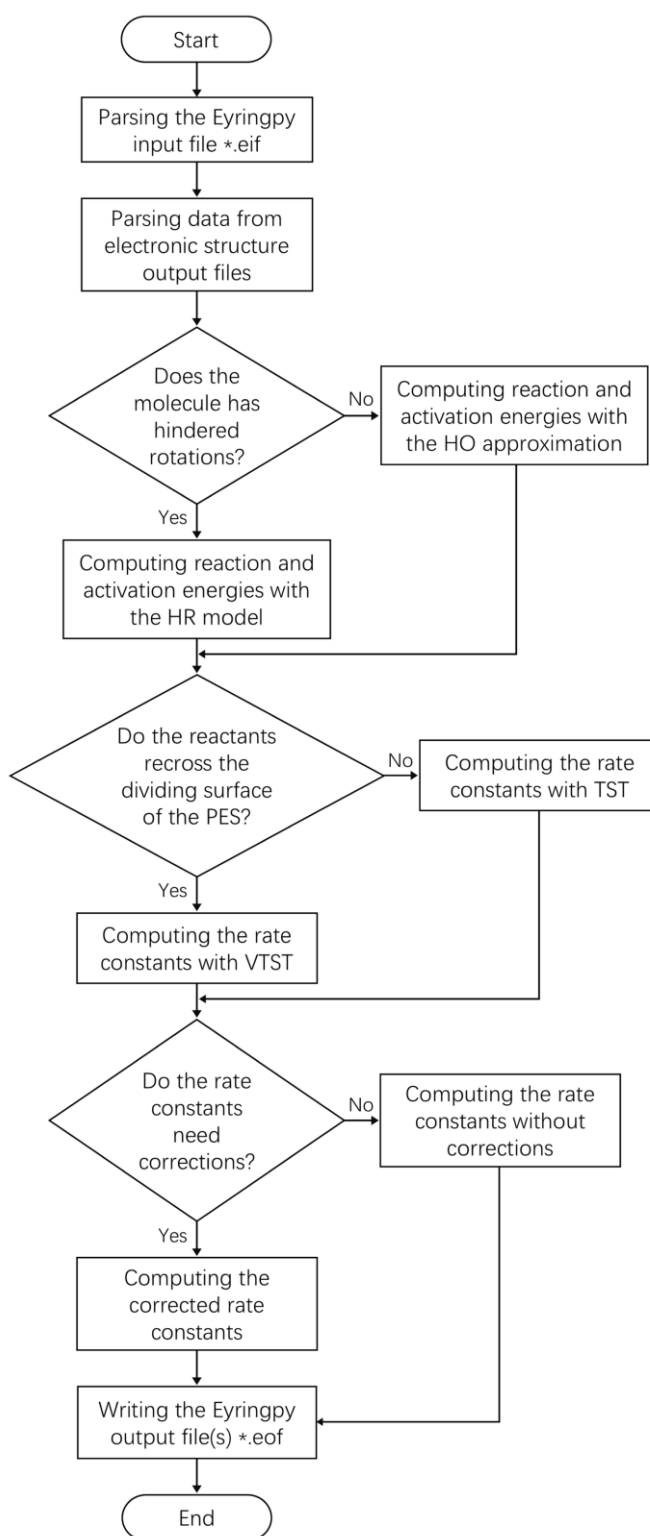


**Figure 2.1** Flowchart of the algorithm for computing rate constants with *Eyringpy*.

### Variational transition state theory

Let us discuss the *Eyringpy* algorithm to compute VTST rate constants. A VTST calculation requires the following data along the MEP: (1) the potential energy, (2) the frequencies, (3) the moments of inertia, and (4) the symmetry numbers. The MEP is obtained by computing the IRC<sup>104,105</sup> with an electronic structure software. The IRC, in isoinertial coordinates, is calculated starting from the fully optimized saddle point geometry and then moving downhill to reactants and products. The step size is one of the main parameters determining the reliability of the IRC. It should be chosen according to the potential energy profile behavior. Curved reaction paths require small step sizes, while flat reaction paths require large ones. If the step size is selected incorrectly, obtaining the MEP that connects the desired reactants and products may be difficult or impossible.<sup>24</sup> For VTST, this may lead to the misidentification of the position of the generalized TS along the MEP and, consequently, to inaccurate rate constants.

Only a fraction of the points along the IRC is necessary to compute VTST rate constants.<sup>26,106</sup> For many decades, the selection of these points has been done manually. Of course, the GTS that minimizes the recrossing can be lost in the process. For this reason, we developed an algorithm, based on the reaction force analysis (RFA) proposed by Toro-Labbé,<sup>107</sup> to automatically choose the points along the IRC that are relevant for VTST. Firstly, *Eyringpy* extracts the reaction coordinate and the electronic energy of each IRC point to build the MEP. The saddle point is placed at  $s = 0$ , the reactants at  $s < 0$ , and the products at  $s > 0$ . The zero of energy is put at the reactants. Subsequently, the reaction force  $F$  is

calculated as the negative gradient of the potential energy  $E(s)$  along the reaction coordinate  $s$ ,

$$F(s) = -\frac{\partial E(s)}{\partial s}. \quad (2.1)$$

The reaction force has a minimum and a maximum at the inflexion points of  $E(s)$ ,  $\alpha$  and  $\gamma$ , respectively, and is zero at the reactants, TS, and products (see Figure 2.2). These points define three zones along  $s$ :  $A \rightarrow \alpha$ ,  $\alpha \rightarrow \gamma$ , and  $\gamma \rightarrow B$ . The first, the “reactant zone”, is characterized by structural changes (*e.g.*, bond stretching, angle bending, rotations, etc.) in the reactants. In the second, the “TS zone,” the main electronic effects occur (*i.e.*, bond breaking and formation). The third, the “product zone,” structural changes also occur.

So, *Eyringpy* chooses the IRC points located in the TS zone (not including the saddle point). The resulting number of points is small, and they are no longer arbitrary. Besides, reducing the number of points can represent a significant saving in the computational cost. Then, *Eyringpy* creates the *Gaussian* input files for the frequency analysis of the selected points. To access to this option of the code, it is necessary to provide the key-value pair METHOD VTST, the IRC output filename(s) through the keyword IRC, and keyword line to perform the frequency analysis with *Gaussian* by the keyword IRCPOINTS\_INP.

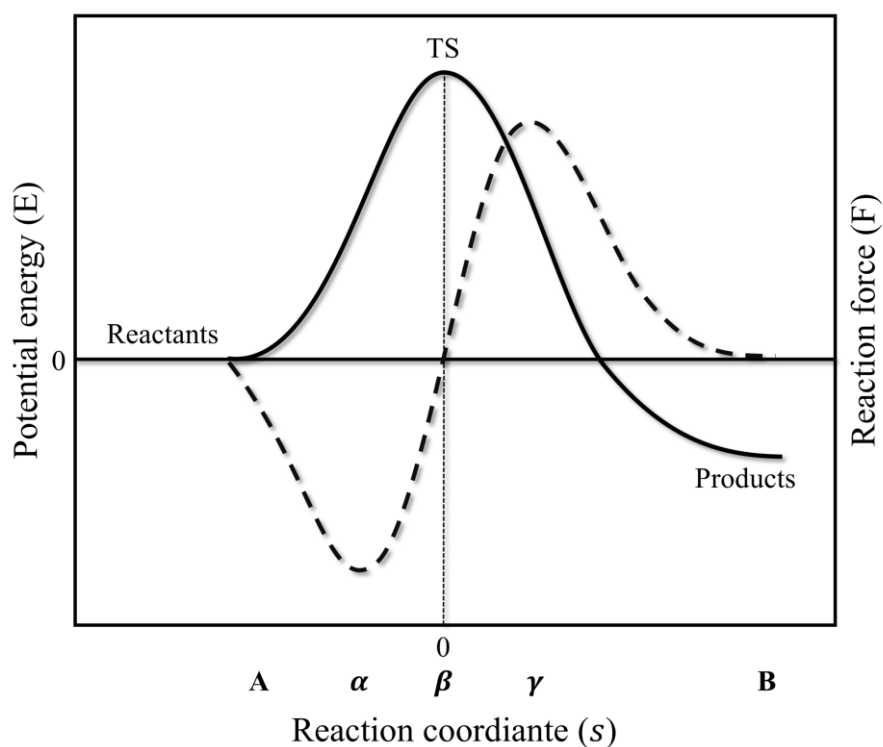


**Figure 2.2** Potential energy (solid line) and reaction force (dashed line) along the reaction coordinate. The points  $\alpha$ ,  $\beta$ , and  $\gamma$  are the minimum, zero, and maximum of the reaction force.

To obtain the VTST rate constants, *Eyringpy* calculates the Gibbs energy at different temperatures<sup>49</sup> of the isolated reactants, the TS and the chosen nonstationary points. The Gibbs energy profile along  $s$  is built with the saddle point at  $s = 0$  and the zero of Gibbs energy at the reactants. Hence, the variational TS is located at the point with the maximum Gibbs activation energy for a given temperature (Eq. 1.3). At the end, *Eyringpy* computes de VTST rate constants with Eq. 1.4. In this case, it is mandatory to use the key-value pair METHOD VTST and the directory's name containing the frequency analysis output files of

the chosen points using the keyword IRCPOINTS. If the points are selected manually, it is also needed to provide the reaction coordinate of each point using the keyword RXCOORD.

### **Hindered rotor model**

As discussed in Chapter 1, a way to improve the accuracy of the Gibbs activation energy is *via* the HR model. The identification of the rotating fragments and the determination of the HR parameters (*i.e.*, the reduced moment of inertia  $I_r$ , the torsional frequency  $\nu_\tau$ , the torsional barrier  $V_0$ , and the total number of minima along the torsional potential  $M$ ) are crucial to apply this method. A common practice is to identify the HRs by visual inspection of the normal modes of vibration. However, this technique depends on the user's experience and can require a lot of time. To carry out this task automatically, some programs have been developed.<sup>11</sup> But, only *Gaussian* is capable of identifying the internal rotors and calculating the input data for the 1D-HR models (*e.g.*, PG and AS schemes). Thus, we build a tool to parse this information from the *Gaussian* output files. It is also important to mention that previous to implement the code it was necessary to derive by hand most of the HR equations because only a few of them has been published in literature.<sup>8,84</sup> The *Sympy* library was employed to verify the polynomials  $P_3$  and  $P_4$  (Table A3, Appendix A) were correct.

The HR algorithm is described as follows. First, the HR parameters are obtained. The torsional potential is calculated with the Eq. 1.29. However,  $\nu_\tau$ ,  $I_r$ , and  $M$  can be extracted from the *Gaussian* output files with the HR analysis of the species with torsions or from the *Eyringpy* input file (*i.e.*, the user can obtain the data with other software). In the second case, the HR parameters must be given using the keywords RED\_MOM\_INERT\_ $x$ , TORFREQ\_ $x$ ,

---

and TORNSYM\_ $x$  (where  $x$  can be R $n$ , RC, TS, P, or P $n$ ; and  $n$  can be 1 or 2 depending on the molecularity of the reaction). Second, the partition function (PG, Eq. 1.23, and AS, Eq. 1.28) and thermodynamic properties (PG, Tables 1.2-1.3, and AS, Table 1.4) of the hindered rotor are calculated. Third, the vibrational component to the partition function (Eq. 1.12) and the thermodynamic properties are calculated (Table A2, Appendix A). Finally, the resulting total partition function (Eq. 1.14) and the thermodynamic properties are obtained (Table A2, Appendix A). The chosen HR model (PG or AS) must be supplied with the keyword HINDROT.

### Reaction symmetry

The rate constants including the reaction symmetry are computed by Eq. 1.36 (TST) and Eqs. 1.4 and 1.36 (VTST). The symmetry numbers for external rotation  $\sigma$  are removed from the partition functions (Tables A1, Appendix A). When the HR model is used, the torsional symmetry numbers  $\sigma_{\tau}$  are also eliminated from the HR partition function (PG, Eq. 1.23, and AS, Eq. 1.28). The reaction symmetry number  $\sigma_{Rx}$  must be provided by the keyword RXSYM. Otherwise, a  $\sigma_{Rx} = 1$  is employed. The calculation of  $\sigma_{Rx}$  is explained in Chapter 2. The thermochemistry considering the symmetry numbers is also offered. By default, the symmetry numbers (external and internal) are extracted from the frequency analysis output files of the molecules involved in the reaction. Alternatively, if the geometry are optimized without symmetry, the symmetry numbers for external rotation must be provided with the keywords NSYM\_R $n$ , NSYM\_RC, NSYM\_TS, NSYM\_P $n$ , and NSYM\_PC ( $n$  can take values of 1 or 2 depending on the molecularity of the reaction).

### Pre-reactive and product complexes

The rate constants for reactions with pre-reactive complexes are calculated as the product of the equilibrium constant between the reactants and the pre-reactive complex,  $K_1$  (Eq. 1.39), and the rate constant of the second step,  $k_2$ . However, for TST the Gibbs activation energy of the second step is obtained with respect to the TS (Eq. 1.40) while in the case of VTST the GTS is used (Eq. 1.41). Furthermore, if tunneling is involved the RC should be considered if and only if its energy is lower when compared to the isolated reactants. In this case, the tunneling barriers are computed (enthalpies of activation at 0 K for the forward and reverse directions) with respect to the energies of the pre-reactive and product complexes. Otherwise, the program employs the energy of the isolated reactants.<sup>49</sup> The frequency output files of the reactant and product complexes must be given using the keywords RC and PC, respectively.

### Validation

The functionalities and accuracy of the new algorithms implemented in *Eyringpy* to compute rate constants are tested with two gas-phase reactions. On the one hand, the reaction of formic acid with the hydroxyl radical shows the importance of using VTST to treat the recrossing effect that can be present in low-barrier reactions at elevated temperatures. On the other hand, the reaction of methane with hydroxyl radical is used to exemplify how to compute the thermodynamic properties of molecules with torsions. The rate constants computed with *Eyringpy* are compared with the theoretical and experimental values found in

the literature. *KiSThelP*<sup>25</sup> was employed to validate the VTST and reaction symmetry methods because, when compared to the other software available for VTST,<sup>53-55,73</sup> it is easier to install, it needs a lower amount of input data, and implies a lower computational cost. The *TheRate*<sup>26</sup> was used to validate the AS model for the same reasons that *KiSThelP*.<sup>25</sup> The Eckart tunnel and AS modules of the *TheRate*<sup>26</sup> were provided by Prof. Annia Galano.

### Hydrogen abstraction from formic acid by hydroxyl radical

#### Computational details

All geometries were fully optimized at the M05-2X<sup>108</sup>/6-311++G(d,p) level. The nature of all stationary points was determined by performing a harmonic vibrational frequency analysis at the same level. Local minima and TSs were identified by the number of imaginary frequencies, 0 and 1, respectively. Unrestricted computations were used for open-shell systems. The M05-2X functional has been recommended for theoretical kinetic computations by their developers<sup>108</sup> and it has been also used successfully in previous works.<sup>78,109-114</sup> The IRC was carried out to guarantee that the TSs connect the desired reactants and products.<sup>104,105</sup> The MEP was computed starting from the fully optimized TSs and then moving downhill along the reactants and products in mass-weighted internal coordinates. Neither reorientation nor symmetry were used to build the IRC. One hundred points were computed on each side of the TSs, using a step size of 0.05 amu<sup>1/2</sup> bohr. All the computations were done with *Gaussian 09*.<sup>102</sup>

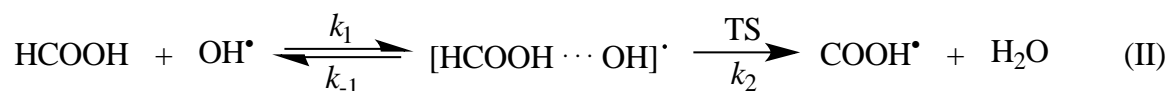
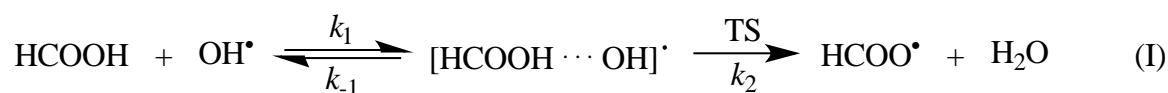
The thermal rate constants were computed by direct dynamics with the TST<sup>1,44</sup> and VTST<sup>5,6,52</sup> as implemented in *Eyringpy*.<sup>24,49,97</sup> Reaction energies and activation barriers were calculated with the HO approximation, including the ZPE. In the VTST algorithm of



*Eyringpy*, the rate constant computations are based on the geometrical and electronic structure data of a set of points along the MEP. These points are in the TS zone and were obtained using the reaction force analysis<sup>107</sup> as implemented in *Eyringpy*.<sup>24</sup> Tunneling factors were computed using the one-dimensional Eckart potential energy barrier.<sup>19</sup>

## Results and discussion

Two principal pathways were studied: (I) the hydrogen abstraction from the carboxyl group and (II) the hydrogen abstraction from the formyl group. Pathway I leads to forming of formyloxyl radical (HCOO·) and water, while pathway II produces hydroxyformyl radical (·COOH) and water. Figure C1 (Appendix C) depicts the fully optimized structures of the reactants and products, involved in both pathways, and their geometrical parameters agree quite well with the reported theoretical<sup>115</sup> and experimental values.<sup>116-118</sup> Both pathways start with forming a pre-reactive complex without a hydrogen transfer barrier prior to the TS, ultimately leading to the formation of the respective products.



Each type of abstraction has two possible pathways. Based on Anglada,<sup>115</sup> neither the double proton transfer nor the addition of hydroxyl radical to formic acid was considered. Figures 2.3 and 2.4 display the energetic profiles of the different reaction pathways. They

also show the fully optimized geometries of the TSs, RCs, and PCs participating in the reaction.

**Acidic hydrogen abstraction.** There are two possible pathways (Ia and Ib) to abstract H from the carboxylic group (Figure 2.3). Both start at the same pre-reactive complex (RC-I). As first discussed by Anglada,<sup>115</sup> pathway Ia takes place, by a proton-coupled electron transfer (PCET) mechanism. Pathway Ib occurs by a hydrogen atom transfer (HAT) from formic acid to the OH radical. Both pathways yield the same product complex (PC-I). The energetically favored mechanism is PCET.

**Formyl hydrogen abstraction.** Two TSs (TS-IIa and TS-IIb) were obtained, which differ by the relative orientation of the OH radical with respect to formic acid (Figure 2.4). In TS-IIa, the OH approaches the hydroxyl oxygen, while in TS-IIb it approaches the carbonyl oxygen. Despite being geometrically different, their  $E_0$  differ by only 0.4 kcal mol<sup>-1</sup>! The rate constants of these pathways have been treated as additive in a previous work.<sup>115</sup> However, in 2011, Iuga, Alvarez-Idaboy, and Vivier-Bunge,<sup>119</sup> showed that TS-IIa and TS-IIb are separated by a very small barrier as a consequence of the nearly free rotation around the O-H bond formed between the OH oxygen and the transferred H atom. Consequently, they concluded that the rate constants of pathways IIa and IIb should not be added. Instead, the one with the higher value should be selected.

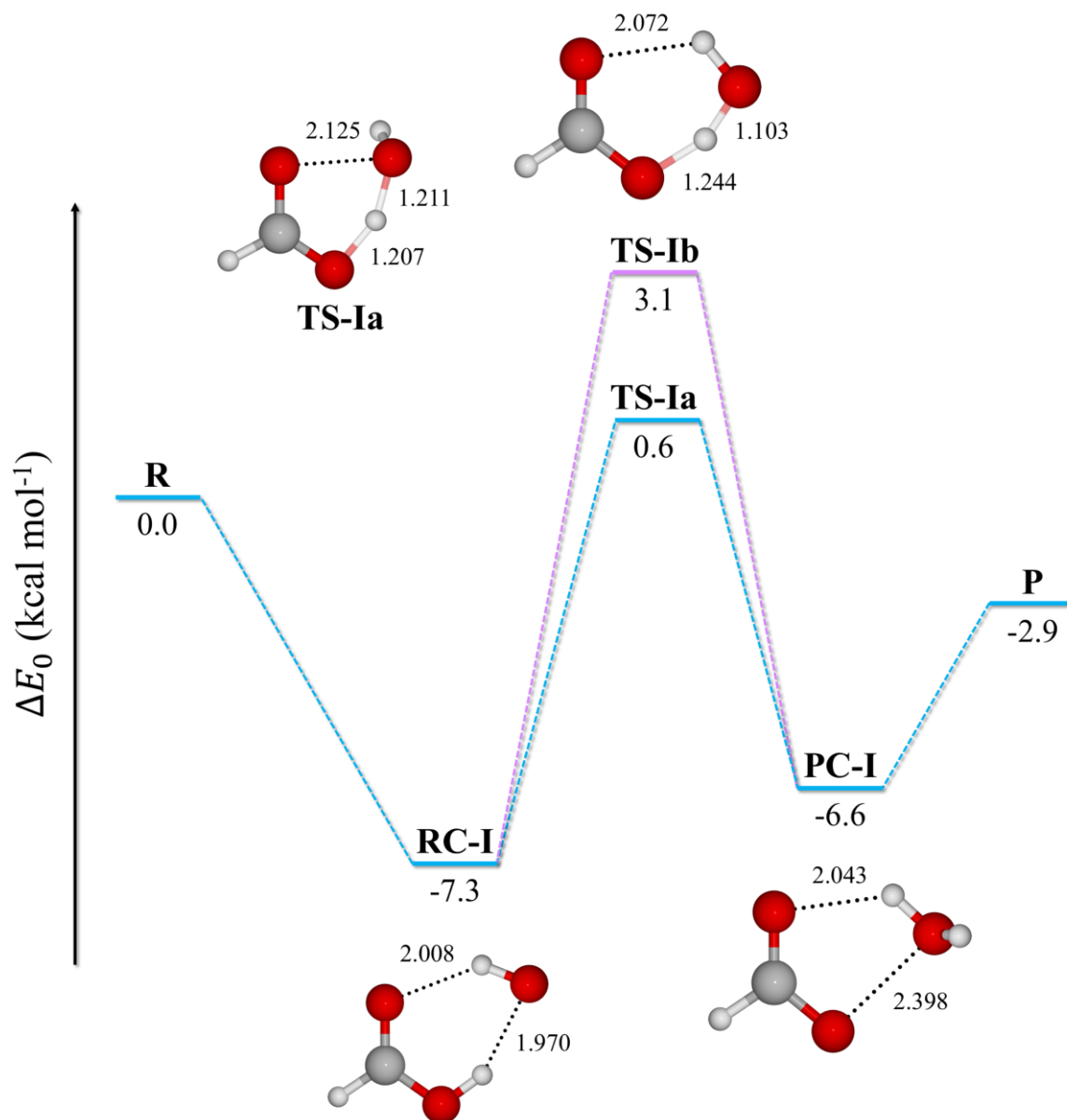


**Figure 2.3** Electronic energy + ZPE profiles (in kcal mol<sup>-1</sup>) of the carboxylic H-abstraction pathways (Ia and Ib) at the M05-2X/6-311++G(d,p) level. Bond lengths are in Angstrom.

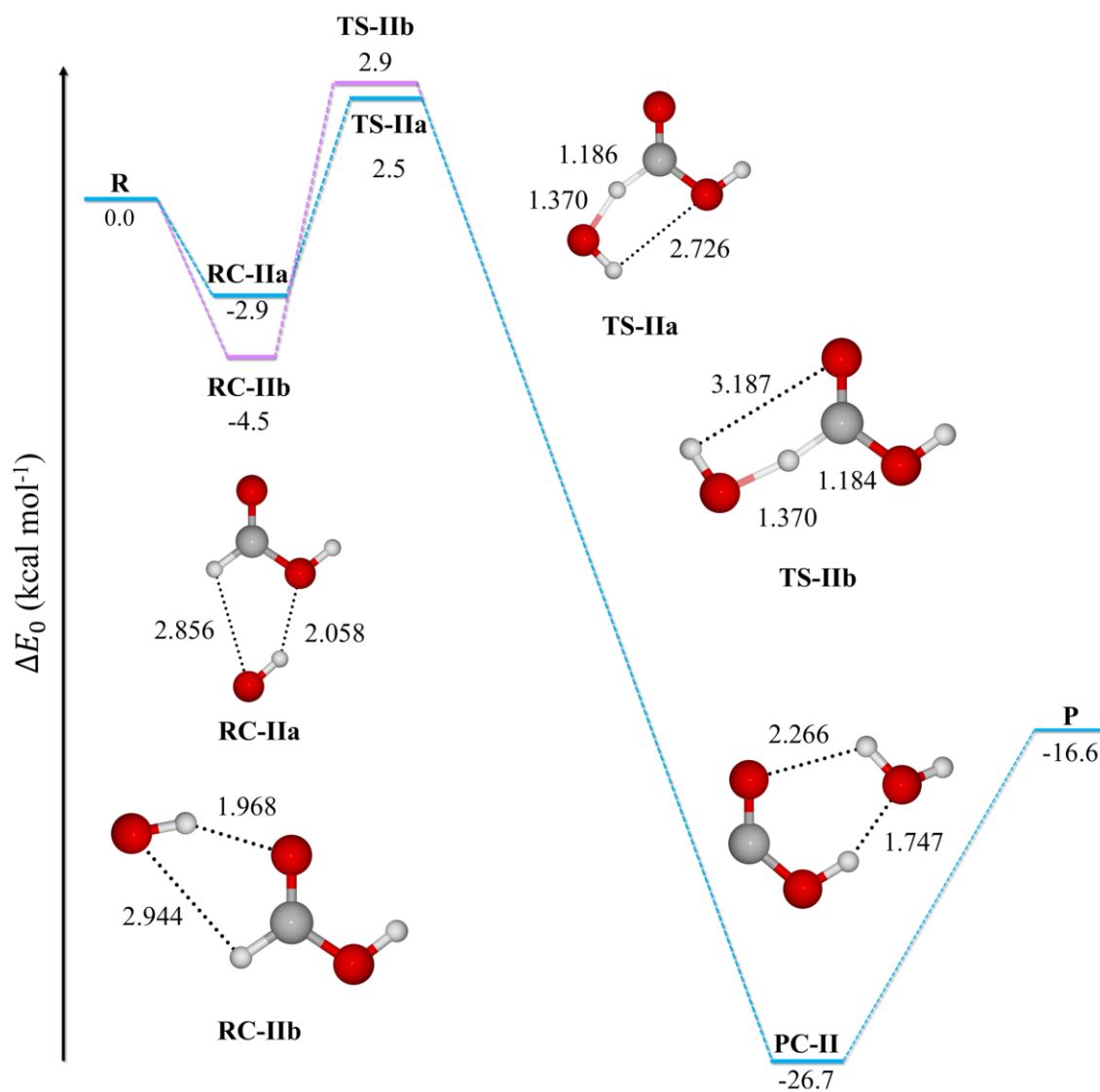


**Figure 2.4** Electronic energy + ZPE profiles (in kcal mol<sup>-1</sup>) of the formyl H-abstraction pathways (IIa and IIb) at the M05-2X/6-311++G(d,p) level. Bond lengths are in Angstrom.

**Kinetics and Branching ratios.** The global rate constant for the reaction of formic acid with hydroxyl radical is obtained as the sum of the rate constants of every path as:

---

$$k_{overall} = k_{Ia} + k_{Ib} + k_{IIa} + k_{IIb} \quad (2.2)$$

Since the reaction studied is of interest under tropospheric conditions,<sup>13,115,119-123</sup> the present discussion will focus on the results obtained in the temperature range of 298.15-440 K. This is the range for which most experimental data is available.<sup>124</sup> The global rate constants for this reaction are reported in Table 2.2 and depicted in Figure 2.5. The calculated values are in excellent agreement with reported theoretical<sup>13,115,119</sup> and experimental values,<sup>120-123</sup> and differ from experiment by a factor of at most 2.6. Moreover, the TST rate constants are given to show the importance of using VTST to compute rate constants. As expected, TST rate constants are overestimated by a factor up to 8.8. However, the agreement improves when VTST is used. Although, this is highly temperature dependent. The recrossing factor (*i.e.*, the ratio  $k_{TST}/k_{VTST}$ ) measures the variational effect in a reaction system. In this case the variational effect is higher with increasing temperature (Table C1, Appendix C).

Table C2 (Appendix A) shows the branching ratios (expressed as a percentage) of the different pathways. Pathway Ia is the most significant contribution to the global rate constant, from 97.1% at 298.15 K to 77.1% at 440 K. Pathway IIb is the smallest contribution, from 0.1% at 298.15 K to 0.8% at 440 K.  $\Gamma_{Ia}$  decreases with increasing temperature but is still the most significant contributor to the global rate constant. Path Ib, has a very small contribution at 298.15 K (2.4%). Nevertheless, its contribution increases up to 19.1% at 440 K.

Remarkably, the VTST rate constants obtained with *Eyringpy* are in perfect agreement with the ones calculated using *KiSThelP*.<sup>25</sup> For computing VTST rate constants,

*Eyringpy* requires only to fill out a simple input file with the output files of the geometric and electronic data of the stationary points and a small set of non-stationary points. The calculation of the VTST rate constants for the present reaction took 1.8 seconds at most.

**Table 2.2** Overall rate constants (in  $\text{cm}^3 \text{molecule}^{-1} \text{s}^{-1}$ ) of the gas phase hydrogen abstraction from formic acid by  $\cdot\text{OH}$  in the 298.15-440 K range.

T (K)	TST	VTST	VTST/ ECK	Theo <sup>13</sup>	Theo <sup>115</sup>	Theo <sup>119</sup>	Exp <sup>120</sup>	Exp <sup>121</sup>	Exp <sup>122</sup>	Exp <sup>123</sup>	<i>KiSThelP</i> <sup>25</sup>
<b>298.15</b>	<b>5.6E-14</b>	<b>3.4E-14</b>	<b>3.4E-13</b>	<b>3.4E-13</b>	<b>6.2E-13</b>	<b>4.5E-13</b>	<b>3.2E-13</b>	<b>4.7E-13</b>	<b>4.9E-13</b>	<b>4.1E-13</b>	<b>3.4E-13</b>
300.00	5.7E-14	3.4E-14	3.3E-13	3.4E-13	6.1E-13	4.4E-13		4.7E-13		4.1E-13	3.3E-13
320.00	6.8E-14	3.8E-14	2.9E-13	3.1E-13	3.6E-13			4.6E-13		4.0E-13	2.9E-13
340.00	8.1E-14	4.0E-14	2.5E-13	2.9E-13				4.6E-13		3.9E-13	2.5E-13
360.00	9.5E-14	4.3E-14	2.2E-13	2.7E-13				4.5E-13		3.9E-13	2.2E-13
380.00	1.1E-13	4.7E-14	2.0E-13	2.5E-13				4.4E-13		3.8E-13	2.0E-13
400.00	1.3E-13	5.1E-14	1.8E-13	2.4E-13				4.4E-13		3.8E-13	1.8E-13
420.00	1.6E-13	5.6E-14	1.7E-13	2.3E-13				4.4E-13		3.7E-13	1.7E-13
440.00	1.9E-13	6.0E-14	1.7E-13	2.2E-13				4.3E-13		3.7E-13	1.7E-13

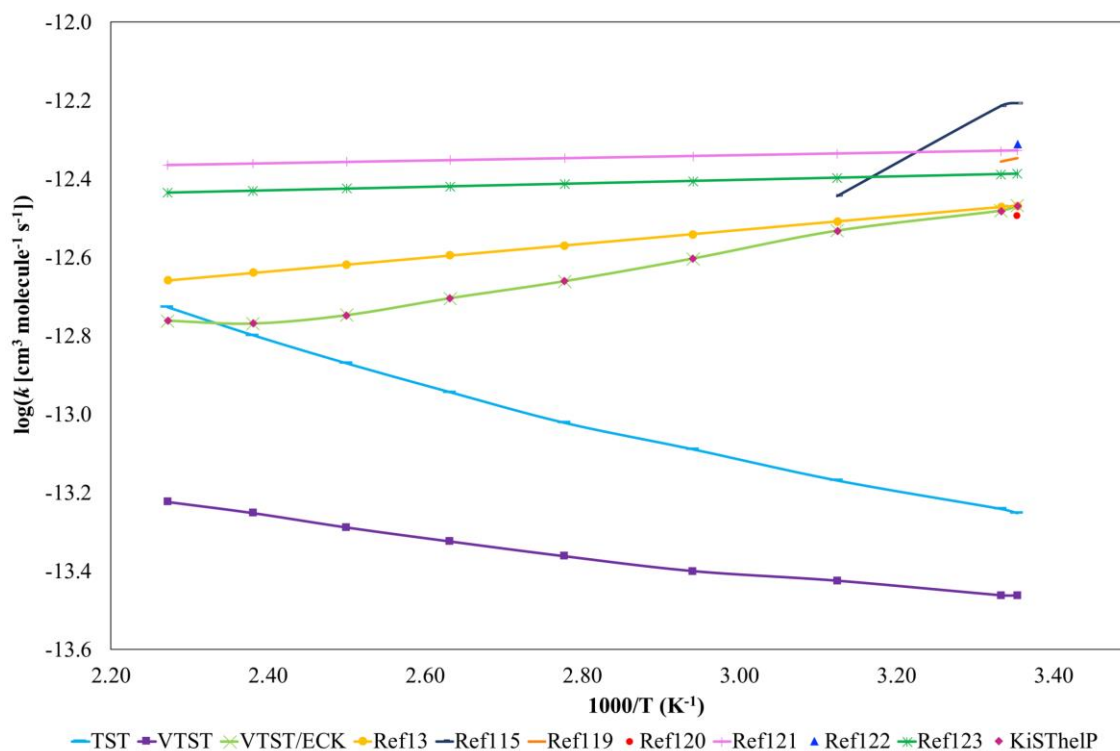


**Figure 2.5.** Overall rate constants (in  $\text{cm}^3 \text{ mol}^{-1} \text{ molecule}^{-1}$ ) of the gas phase hydrogen abstraction from formic acid by  $\cdot\text{OH}$  in the 298.15-440 K range.

## Hydrogen abstraction from methane by hydroxyl radical

### Computational details

Full geometry optimizations were done at the BhandHLYP/6-311G(d,p) level. The nature of all the stationary points was determined by performing a harmonic vibrational frequency analysis at the same level. Local minima and TSs were identified by the number of imaginary frequencies, 0 and 1, respectively. Energies were refined by single point computations at the CCSD(T)/6-311G(d,p) level. Unrestricted computations were used for open-shell systems. The energetic analysis is based on the CCSD(T)/6-311G(d,p)//BhandHLYP/6-311G(d,p) level including the ZPE at the BhandHLYP/6-

311G(d,p) level. The IRC was performed to ensure that the TSs connect the desired reactants and products.<sup>104,105</sup> The MEP was computed starting from the fully optimized TS and then moving downhill along the reactants and products, in mass-weighted internal coordinates. Neither reorientation nor symmetry were employed to build the IRC. One hundred points were computed on each side of the TSs, using a step size of 0.05 amu<sup>1/2</sup> bohr. The HRs and their parameters (torsional frequency, symmetry, and reduced moment of inertia) were determined with the algorithm of Ayala and Schlegel<sup>8</sup> as implemented in *Gaussian 09*.<sup>102</sup> The torsional potential was calculated by a scanning from 0° to 360° in increments of 20°. All the computations were done with *Gaussian 09*.<sup>102</sup>

The thermal rate constants were computed by direct dynamics with the TST<sup>1,44</sup> as implemented in *Eyringpy*.<sup>24,49,97</sup> Tunneling factors were computed using a one-dimensional Eckart potential energy barrier.<sup>19</sup> The partition functions and thermodynamic properties of the low-frequency vibrational modes corresponding to internal rotations were calculated with the one-dimensional models of Pitzer and Gwinn<sup>84</sup> and Ayala and Schlegel<sup>8</sup> as implemented in *Eyringpy*.<sup>97</sup>

### Results and discussion

The calculated thermal rate constants for this reaction in the 298.15-650 K temperature range are listed in Table 2.3 and shown in Figure 2.6. Vibrational modes are considered as harmonic oscillators except for the rotation of the -CH<sub>3</sub> group of the TS, which is treated as a hindered rotation. The torsional frequency is 54.15 cm<sup>-1</sup> and the torsional barrier is 0.4 kcal mol<sup>-1</sup>. Note the tunnel effect is neglected, TST rate constants are underestimated by up to 2 orders of magnitude. Hence, this shows the importance of using a

---



correction factor when a reaction proceeds through mechanisms in which there is transference of light particles, such as the hydrogen radical. Regarding the treatment of vibrations, it is clear the TST values are in better agreement with experiment when the HR approximation is used. However, due to the barrier for the  $-\text{CH}_3$  rotation being lower than RT, the improvement of the TST values is low. The ratio  $k_{TST}^{HO}/k_{TST}^{HR}$  goes from 1.1 at 298.15 K to 1.4 at 650 K for both PG and AS hindered rotor models.

**Table 2.3** Rate constants (in  $\text{cm}^3 \text{ molecule}^{-1} \text{ s}^{-1}$ ) as function of temperature of the hydrogen abstraction from  $\text{CH}_4$  by  $\cdot\text{OH}$  in the gas phase.

T(K)	TST/HO	TST/PG	TST/AS	TST/PG/ECK	TST/AS/ECK	Theo <sup>125</sup>	Exp <sup>126</sup>	TheRate <sup>26</sup>
298.15	7.90E-17	7.20E-17	7.30E-17	3.70E-15	3.70E-15	2.00E-15	6.33E-15	3.70E-15
300	8.60E-17	7.80E-17	7.90E-17	3.80E-15	3.90E-15	2.07E-15	6.58E-15	3.90E-15
320	2.00E-16	1.80E-16	1.80E-16	5.30E-15	5.30E-15	2.93E-15	9.76E-15	5.30E-15
340	4.20E-16	3.70E-16	3.70E-16	7.30E-15	7.30E-15	4.12E-15	1.40E-14	7.30E-15
360	8.20E-16	7.00E-16	7.10E-16	9.90E-15	1.00E-14	5.73E-15	1.94E-14	1.00E-14
380	1.50E-15	1.30E-15	1.30E-15	1.30E-14	1.40E-14	7.87E-15	2.63E-14	1.40E-14
400	2.60E-15	2.20E-15	2.20E-15	1.80E-14	1.80E-14	1.07E-14	3.48E-14	1.80E-14
450	8.60E-15	6.80E-15	6.90E-15	3.60E-14	3.60E-14	2.14E-14	6.47E-14	3.60E-14
500	2.30E-14	1.70E-14	1.80E-14	6.70E-14	6.70E-14	3.96E-14	1.10E-13	6.70E-14
550	5.30E-14	3.90E-14	3.90E-14	1.20E-13	1.20E-13	6.81E-14	1.75E-13	1.20E-13
600	1.10E-13	7.60E-14	7.70E-14	1.90E-13	2.00E-13	1.10E-13	2.62E-13	2.00E-13
650	2.00E-13	1.40E-13	1.40E-13	3.00E-13	3.10E-13	1.70E-13	3.77E-13	3.10E-13

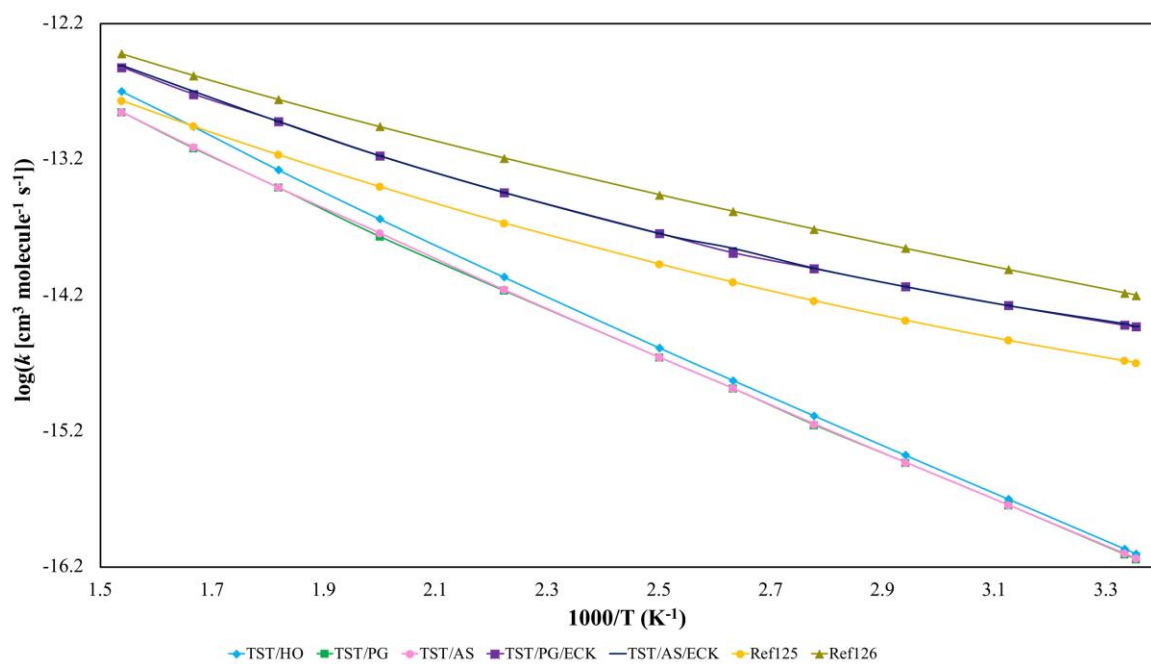


**Figure 2.6** Overall rate constants (in  $\text{cm}^3 \text{ molecule}^{-1} \text{ s}^{-1}$ ) as function of temperature of the hydrogen abstraction from  $\text{CH}_4$  by  $\cdot\text{OH}$  in the gas phase.

### 3 Conclusions

We implemented four new methods to improve the accuracy of the rate constants estimated with *Eyringpy*. We use the variational transition state theory to minimize the recrossing effects. An algorithm, based on the reaction force analysis, was designed to select automatically the relevant non-stationary points along the MEP for computing VTST rate constants. As expected, the resulting number of points is small. This is very useful because it significantly reduces the computational cost. We included the models of Pitzer-Gwinn and Ayala-Schlegel to obtain more accurate reaction and activation energies of molecules internal rotations. An algorithm to calculate the tunneling barriers for bimolecular reactions with pre-reactive complexes was designed. Finally, the effect of the reaction path degeneracy was implemented. Besides, the *Eyringpy* binaries (for *Windows*, *Linux*, and *macOS X*) were built to distribute it as a stand-alone, multiplatform, and easy-to-install program. Other improvements are the compatibility of the code with several versions of *Gaussian* and the fixing of several bugs.

To evaluate the effectiveness and accuracy of the new algorithms implemented in *Eyringpy* two gas phase reactions were used. The calculated rate constants of both reactions are in better agreement when compared to the experimental values. Besides, the *Eyringpy* results are in perfect agreement with *KiSThelP* and *TheRate*. Highlights of *Eyringpy*, other than being free of charge, are its user-friendliness, easy installation, and low computing time.

---

**Appendix A Contributions to the canonical partition functions and thermodynamic properties.**

**A1. Contributions to the canonical partition function.**

Contribution	Partition function
<b>Translational</b>	$q_{trans} = \left(\frac{2\pi mk_B T}{h^2}\right)^{\frac{3}{2}} \frac{k_B T}{P}$
<b>Rotational linear</b>	$q_{rot}^l = \frac{T}{\sigma \theta_{rot}}, \quad \theta_{rot} = \frac{\hbar^2}{2Ik_B}$
<b>Rotational nonlinear</b>	$q_{rot}^{nl} = \frac{\pi^{1/2}}{\sigma} \left[ \frac{T^{3/2}}{(\theta_{rotA} \theta_{rotB} \theta_{rotC})^{1/2}} \right], \quad \theta_{rotj} = \frac{\hbar^2}{2I_j k_B}, \quad j = A, B, C$
<b>Vibrational</b>	$q_{vib} = \prod_{i=1}^{n_v^{[a]}} \frac{e^{-\theta_{vib_i}/2T}}{1 - e^{-\theta_{vib_i}/T}}, \quad \theta_{vib_i} = \frac{h\nu_i}{k_B}$
<b>Electronic</b>	$q_{elec} = \omega_0$

---

<sup>[a]</sup> The number of vibrational modes  $n_v$  is  $3N - 5$  or  $3N - 6$  for linear and nonlinear molecules, respectively, where  $N$  is the number of atoms.

**Table A2.** Thermodynamic properties per mole of substance.

<b>Internal energy</b>	$U = RT^2 \left( \frac{\partial \ln q}{\partial T} \right)_{N,V}$
<b>Entropy</b>	$S = R \left[ \left( \frac{\partial \ln q}{\partial T} \right)_V T + \ln q \right]$
<b>Enthalpy</b>	$H = RT \left[ \left( \frac{\partial \ln q}{\partial T} \right)_V T + 1 \right]$
<b>Gibbs energy</b>	$G = -RT \ln q$

---

---

**Table A3.** Polynomials for the hindered rotor model of Ayala and Schlegel.

---

$$\begin{aligned} P_1 = & 0.003235x - 0.026252x^2 + 0.110460x^3 - 0.203340x^4 + 0.130633x^5 - 0.010112y^{\frac{1}{2}} \\ & + 0.650122xy^{\frac{1}{2}} + 0.067112x^2y^{\frac{1}{2}} + 0.088807x^3y^{\frac{1}{2}} - 0.014290x^4y^{\frac{1}{2}} - 0.364852y \\ & + 0.913073xy - 0.021116x^2y - 0.092086x^3y - 0.415689y^{\frac{3}{2}} - 1.128961xy^{\frac{3}{2}} \\ & + 0.223009x^2y^{\frac{3}{2}} + 0.421344y^2 + 0.505139xy^2 - 0.215088x^2y^{\frac{5}{2}} \end{aligned}$$

$$\begin{aligned} P_2 = & 0.067113x + 0.772485x^2 - 3.0674131x^3 + 4.595051x^4 - 2.101341x^5 + 0.015800y^{\frac{1}{2}} \\ & + 0.102119xy^{\frac{1}{2}} - 0.555270x^2y^{\frac{1}{2}} - 1.125261x^3y^{\frac{1}{2}} + 0.071884x^4y^{\frac{1}{2}} - 0.397330y \\ & + 2.284956xy + 0.850046x^2y - 0.174240x^3y - 0.451875y^{\frac{3}{2}} - xy^{\frac{3}{2}} \\ & - 2.136226xy^{\frac{3}{2}} + 0.303469x^2y^{\frac{3}{2}} + 0.470837y^2 + 0.675898xy^2 \end{aligned}$$

$$\begin{aligned} P_3 = & -0.3265825x^5 + 0.035725x^4y^{\frac{1}{2}} + 0.406668x^4 - 0.177614x^3y^{\frac{1}{2}} + 0.230215x^3y - 0.16569x^3 \\ & - 0.100668x^2y^{\frac{1}{2}} + 0.042232x^2y - 0.5825225x^2y^{\frac{3}{2}} + 0.026252x^2 - 0.650122xy^{\frac{1}{2}} \\ & + 1.2628475xy^2 - 1.3696095xy + 2.257922xy^{\frac{3}{2}} - 0.0016175x + 0.005056y^{\frac{1}{2}} \\ & - 0.842688y^2 + 0.364852y + 0.6235335y^{\frac{3}{2}} + 0.53772y^{\frac{5}{2}} \end{aligned}$$

$$\begin{aligned} P_4 = & 5.2533525x^5 - 0.17971x^4y^{\frac{1}{2}} - 9.190102x^4 + 2.250522x^3y^{\frac{1}{2}} + 0.4356x^3y + 4.60111965x^3 \\ & + 0.832905x^2y^{\frac{1}{2}} - 1.700092x^2y - 0.7586725x^2y^{\frac{3}{2}} - 0.772485x^2 - 0.102119xy^{\frac{1}{2}} \\ & - 1.689745xy^2 - 3.427434xy + 4.272452xy^{\frac{1}{2}} - 0.0335565x - 0.0079y^{\frac{1}{2}} \\ & - 0.941674y^2 + 0.39733y + 0.6778125y^{\frac{3}{2}} + 0.56577175y^{\frac{5}{2}} \end{aligned}$$

---

---

## Appendix B *Eyringpy* user's manual

### B1 Software requirements

*Eyringpy* is a command-line program written in *Python3*. It is compatible with *Windows*, *Linux*, and *macOS X*, and is distributed as a stand-alone executable. *Eyringpy* requires the output files of *Gaussian* (*09*<sup>102</sup> or *16*<sup>38</sup>) (\*.out or \*.log) with the frequency analysis of the species involved in the reaction (reactant(s), product(s), TSs, and RCs and/or PCs, if necessary), and/or with the IRC data. Besides, the *Eyringpy*'s input file (foldername.eif) is also needed. It is not mandatory to install *Eyringpy* in the same computer where *Gaussian* is running. For more information about *Gaussian*, visit its web page: <https://www.gaussian.com>. *Eyringpy* can be downloaded from <https://www.theochemmerida.org/eyringpy>.

### B2 Installing *Eyringpy*

The installation of *Eyringpy* is simple and straightforward. However, if you have problems installing it, contact us for assistance at [eyringpy2018@gmail.com](mailto:eyringpy2018@gmail.com). To install *Eyringpy* you have to go through the steps for the operating system you chose.

#### B2.1 Windows

1. Download the `eyringpyversion_windows_xbits.zip` file, move it to the directory of your choice, and decompress it.
2. Open the command prompt (`cmd` or `cmd.exe`):
  - \* Press Win+R to open the run box, type `cmd`, and press Enter.

**Note:** For detailed information about the commands, please visit:

---

<https://docs.microsoft.com/en-us/windows-server/administration/windows-commands/windows-commands>.

3. Go to the `eyringpyversion_windows_xbits` directory:

```
> cd path-to-eyringpyversion_windows_xbits-directory
```

**Example:**

```
> cd Documents\Programs\eyringpy3.0_windows_64bits
```

4. Type `dir /s` to display all the files and subdirectories in the `eyringpyversion_windows_xbits` directory and make sure it has the directories `bin`, `manual`, and `test`.

5. Add an *Eyringpy* alias (e.g. `eyringpy`) to a Batch script to run the program in any directory:

- \* Open notepad (by the graphical user interface (GUI) or type `notepad` in the `cmd` and press `Enter`) and paste the lines shown in Figure B1.

```
@echo off
title command prompt
doskey eyringpy=path-to-eyringpyversion_windows_xbits-directory\bin\eyringpy.exe $1
```

**Figure B1.** Batch script (`profile.bat`) to generate the *Eyringpy* alias in *Windows*.

**Example:**

```
doskey          eyringpy=          C:\Users\Eugenia\Documents\Programs
\eyringpy3.0_windows_64bits\bin\eyringpy.exe $1
```

- \* Save the file as `profile.bat` in the Desktop or in Documents.

**Note:** To edit the `profile.bat` file, right-click on its icon and select `Edit`.

- 
- \* Create a desktop shortcut of the cmd.
  - \* Right-click the cmd shortcut, select Properties from the menu, and click the Shortcut tab.
  - \* In the Target field, type path-to-cmd.exe /k path-to-profile.bat and click Ok.

**Example:**

Target:                   %windir%\system32\cmd.exe                   /k  
C:\Users\Eugenia\Desktop\profile.bat

**Note:** For more information about the doskey command and Batch scripts please visit:  
<https://docs.microsoft.com/en-us/windows-server/administration/windows-commands/doskey>                   and                   <https://docs.microsoft.com/en-us/azure/devops/pipelines/tasks/utility/batch-script?view=azure-devops>,  
respectively.

**6.** Run a test job of *Eyringpy*:

- \* Double-click the cmd Shortcut.
- \* Go to one of the test' subdirectories.

**Example:**

```
> cd  
Documents\Programs\eyringpy3.0_windows_64bits\test\kinetics\gas\g09\hc  
ooh_oh
```

- \* Type the *Eyringpy* alias. If the installation is successful, the *Eyringpy* welcome-help message (Figure B2) will be displayed.



---

```
Eyringpy version 3.0
Authors: Eugenia Dzib, Alan Quintal, Filiberto Ortiz-Chi, and Gabriel Merino
Cinvestav Merida, 2022

Modules

* Kinetics computes rate constants in the gas phase and in solution

To run this module: eyringpy -kin

* IRC-analysis monitors the evolution of primitive changes along the IRC

To run this module: eyringpy -irc

Please check the parameters in the input file foldername.eif
```

**Figure B2.** *Eyringpy* welcome-help message.

Note: The *Eyringpy* welcome-help message in Figure B2 is displayed when there is an *Eyringpy* input file in the current working directory. Otherwise, the last line in the welcome-help message is replaced by “If an input file is required, please run eyringpy -kin or eyringpy -irc as the case may be.”

- \* Type eyringpy -kin or eyringpy -irc depending on the type of computation you choose.
- \* Type dir to list the directory contents and make sure the *Eyringpy* output file foldername.eof is present.
- \* Open the output file foldername.eof (by the GUI or type foldername.eof in the cmd and press Enter). If everything is OK, the “Eyringpy terminated normally” legend is written at the end of the file.

---

## B2.2 *Linux* and *macOS X*

1. Download the `eyringpyversion_linux_or_macos_xbits.tar.gz` file.
2. Open the terminal:
  - \* Press `Ctrl+Alt+T` (*Linux*)
  - \* Press `Command+Space` to launch Spotlight and type `terminal.app` (*macOS X*)
3. Move the `eyringpyversion_linux_or_macos_xbits.tar.gz` file to the directory of your choice and decompress it:

```
$ mv eyringpyversion_linux_or_macos_xbits.tar.gz destination_directory
```

```
$ cd destination_directory
```

```
$ tar -xzf eyringpyversion_linux_or_macos_xbits.tar.gz
```
4. Go to the `eyringpyversion_linux_or_macos_xbits` directory:

```
$ cd path-to-eyringpyversion_linux_or_macos_xbits-directory
```
7. Type `ls -R` to display all the files and subdirectories in the `Eyringpyversion_linux_or_macos_xbits` directory and make sure it has the directories `bin`, `manual`, and `test`.
5. Add the *Eyringpy* path to the `PATH` environment variable to run *Eyringpy* in any directory.
  - \* For *Linux* (bash/sh shell):
    - Open the `.bashrc` file with a text editor (*e.g.* `vi` or `emacs`):

```
$ vi ~/.bashrc
```
    - Add `export PATH="path-to-bin-directory:$PATH"` to the file and save it.

- 
- Reload the .bashrc file

```
$ source ~/.bashrc
```

- \* For *Linux* (csh/tcsh shell):

- Open the .cshrc file with a text editor (*e.g.* vi or emacs):

```
$ vi ~/.cshrc
```

- Add `setenv PATH $PATH:"path-to-bin-directory"` to the file and save it.

- Reload the .cshrc file

```
$ source ~/.cshrc
```

- \* For *macOS X*:

- Open the .bash\_profile file with a text editor (*e.g.* vi or emacs):

```
$ vi ~/.bash_profile
```

- Add `export PATH="path-to-bin-directory:$PATH"` to the file and save it.

- Reload the .bash\_profile file

```
$ source ~/.bash_profile
```

## 6. Run a test job of *Eyringpy*:

- \* Go to one of the test' subdirectories.

### **Example:**

```
$ cd  
Programs/eyringpyversion_linux_or_macos_xbits/test/kinetics/gas/g09/hcoo  
h_oh
```

- 
- \* Type `eyringpy`. If the installation is successful, the *Eyringpy* welcome-help message (Figure B2) will be displayed.
  - \* Type `eyringpy -kin` or `eyringpy -irc` depending on the kind of computation you choose.
  - \* Type `ls` to list the directory content and make sure the *Eyringpy* output file `foldername.eof` is present.
  - \* Open the output file `foldername.eof` (by the GUI or type `foldername.eof` in the cmd and press Enter). If everything is OK, the “Eyringpy terminated normally” legend is written at the end of the file.

**Note:** Do not perform *Eyringpy* computations in the bin directory.

### **B3 The *Eyringpy* input file**

The input data for *Eyringpy* consists of a set of key-value pairs that are specified in a text file. This is named as the current working directory (*i.e.*, the folder in which the user is currently working in) with the extension `*.eif` (see Figure B3). Comments in the `*.eif` file start with the `#` character and blank lines are ignored. The key-value pairs have the structure: `Keyname Value`. The keywords can appear in any order and are not case-sensitive. Most of them have reliable default values that allow having extremely short input files. Three types of input options are available in *Eyringpy*: general, to compute rate constants, and to monitor the evolution of primitive changes along the IRC. However, in this thesis only the keys related to the new kinetic theories implemented in *Eyringpy* will be described. For each key

---

it will be given its description, type, and format, and, if applicable, its default value, unit, and options.

METHOD	VTST
TUNNEL	ECK
HINDROT	PG
TEMP	200 300 10
REACT1	react1.out
REACT2	react2.out
RC	rc.out
TS	ts.out
PC	pc.out
PROD1	prod1.out
PROD2	prod2.out
RXSYM	4
IRCPOINTS	ircpoints

**Figure B3.** Example of an *Eyringpy* input file.

Let describe the keywords included in *Eyringpy* to compute VTST rate constants with the HR model, RCs, PCs, and reaction symmetry:

- RC: Frequency output filename of the pre-reactive complex. It should be given for reactions where the pre-reactive complex is lower in energy when compared to the reactant(s). If the electronic energy is required at a second level (*e.g.*, MP $n$ , CCSD(T)) the single-point output filename (sp) should be put next to the frequency one.

Type: String

Format: RC rc.out

RC rc.out rc-sp.out

- 
- PC: Frequency output filename of the product complex. It should be given for reactions where the product complex is lower in Gibbs free energy with respect to the product(s). If the electronic energy is required at a second level (*e.g.*, MP $n$ , CCSD(T)) the single-point output filename (sp) should be put next to the frequency one.

Type: String

Format: PC pc.out

PC pc.out pc-sp.out

- \* NSYM\_R $n$ : Rotational symmetry number of the  $n$  reactant, where  $n$  can take the values 1 or 2 depending on the molecularity of the reaction. This key is used when the geometry of the reactant is not symmetrized during the optimization.

Type: Integer

Default value: Rotational symmetry number of the  $n$  reactant obtained by *Eyringpy* from its frequency output file.

Format: NSYM\_R1 12

- \* NSYM\_RC: Rotational symmetry number of the pre-reactive complex. This key is used when the geometry of the pre-reactive complex is not symmetrized during the optimization.

Type: Integer

Default value: Rotational symmetry number of the pre-reactive complex obtained by *Eyringpy* from its frequency output file.

---

Format: NSYM\_RC 6

- \* NSYM\_TS: Rotational symmetry number of the TS. This key is used when the geometry of the TS is not symmetrized during the optimization.

Type: Integer

Default value: Rotational symmetry number of the TS obtained by *Eyringpy* from its frequency output file.

Format: NSYM\_TS 3

- \* NSYM\_PC: Rotational symmetry number of the product complex. This parameter is used when the geometry of the product complex is not symmetrized during the optimization.

Type: Integer

Default value: Rotational symmetry number of the product complex obtained by *Eyringpy* from its frequency output file.

Format: NSYM\_PC 1

- \* NSYM\_Pn: Rotational symmetry number of the  $n$  product, where  $n$  can take the values 1 or 2. This parameter is used when the geometry of the product is not symmetrized during the optimization.

Type: Integer

Default value: Rotational symmetry number of the  $n$  product obtained by *Eyringpy*

---

from its frequency output file.

Format: NSYM\_P1 6

- \* RXSYM: Reaction symmetry or degeneracy path.

Type: Integer

Default value: 1

Format: RXSYM 4

- METHOD: Method to compute rate constants with *Eyringpy*.

Type: String

Default value: TST

Options: TST, VTST\*

Format: METHOD VTST

Note: \* New option included.

- HINDROT: Hindered rotor model.

Type: String

Options: PG, AS

Format: HINDROT PG

- TEMP: Temperature. It can be given as a range (initial, final, and step) or a list.

Type: Float



---

Default value: In the gas phase is 298.15 K. However, in solution temperature does not have a default value due to the solvent viscosity varies with temperature.

Units: Kelvin

Format: TEMP 100 500 10

TEMP\* 100 200 300 400 500

Note: \* New format included.

- STEMP: Special temperature provided as a list. Such temperature(s) is/are added to the values introduced by the keyword TEMP.

Type: Float

Format: STEMP 298.15 316.4 456.3

- \* IRCPOINTS: Directory containing the *Gaussian* output files, with the electronic energy and frequency analysis, of each snapshot along the IRC. It is mandatory for computing VTST rate constants. The outputs must be named according to the forward direction of the IRC (*i.e.*, from reactants to products) as 0001.out, 0002.out, 0003.out, etc. and stored in a directory within the current working directory (cwd). *Eyringpy* has a script to create a directory (called ircpoints) with the *Gaussian* input files of each point of the IRC. The code names the inputs as 0001.inp, 002.inp, 0003.inp, etc. To turn on this option only the following keys must be present in the \*.eif file: METHOD, IRC, REACT $n$ , PROD $n$ , and TS. Furthermore, METHOD must have the value VTST.

---

Type: String

Format: IRCPOINTS cwd/ircpoints

- \* IRCPOINTS\_INP: Set of keywords needed in the *Gaussian* input file(s) (\*.inp) to perform the frequency analysis of each snapshot of the IRC. Four values are required in the next order: memory, functional, basis, freq, and other optional keys (e.g., Nosymm). It can be activated only if the IRC key is present. The inputs are named according to the forward direction of the IRC (i.e., from reactants to products) as 0001.inp, 0002.inp, 0003.inp, etc. and stored in the directory cwd/nbo\_inp.

Type: String

Format: IRCPOINTS\_INP 8GB BHandHLYP aug-cc-pVDZ Freq Nosymm

- \* RXCOORD: Reaction coordinate of each point along IRC for VTST. The value for TS ( $s = 0.0$ ) is introduced automatically by *Eyringpy*.

Type: Float

Units: Bohr (mass-scaled) or  $\text{amu}^{1/2}$  Bohr (mass-weighted).

Default value: Reaction coordinate of each snapshot extracted by *Eyringpy* from the *Gaussian* output file with the electronic energy and frequency analysis. It is important to highlight *Eyringpy* parses this value from the IRC and writes it in the *Gaussian* input files \*.inp.

Format: RXCOORD -0.3 -0.2 -0.1 0.1 0.2 0.3

- 
- TORFREQ\_Rn: Torsional frequencies of the  $n$  reactant for the HR model.  
Type: Float  
Units:  $\text{cm}^{-1}$   
Default value: Torsional frequencies of the  $n$  reactant extracted by *Eyringpy* from the *Gaussian* output file with the frequency and HR analysis.  
Format: TORFREQ\_R1 89.2467 100.6895
  - TORFREQ\_RC: Torsional frequencies of the pre-reactive complex for the HR model.  
Type: Float  
Units:  $\text{cm}^{-1}$   
Default value: Torsional frequencies of the pre-reactive complex extracted by *Eyringpy* from the *Gaussian* output file with the frequency and HR analysis.  
Format: TORFREQ\_RC 89.2467 100.6895
  - TORFREQ\_TS: Torsional frequencies of the TS for the HR model.  
Type: Float  
Units:  $\text{cm}^{-1}$   
Default value: Torsional frequencies of the TS extracted by *Eyringpy* from the *Gaussian* output file with the frequency and HR analysis.  
Format: TORFREQ\_TS 89.2467 100.6895
  - TORFREQ\_PC: Torsional frequencies of the product complex for the HR model.
-

---

Type: Float

Units:  $\text{cm}^{-1}$

Default value: Torsional frequencies of the product extracted by *Eyringpy* from the *Gaussian* output file with the frequency and HR analysis.

Format: TORFREQ\_PC 89.2467 100.6895

- TORFREQ\_Pn: Torsional frequencies of the  $n$  product for the HR model.

Type: Float

Units:  $\text{cm}^{-1}$

Default value: Torsional frequencies of the  $n$  product extracted by *Eyringpy* from the *Gaussian* output file with the frequency and HR analysis.

Format: TORFREQ\_P1 89.2467 100.6895

- RED\_MOM\_INERT\_Rn: Reduced moment(s) of inertia of the  $n$  reactant for the HR model.

Type: Float

Units:  $\text{amu Bohr}^2$

Default value: Reduced moment(s) of inertia of the  $n$  reactant extracted by *Eyringpy* from the *Gaussian* output file with the frequency and HR analysis.

Format: RED\_MOM\_INERT\_R1 89.2467 100.6895

- RED\_MOM\_INERT\_RC: Reduced moment(s) of inertia of the pre-reactive complex

---

for the HR model.

Type: Float

Units: amu Bohr<sup>2</sup>

Default value: Reduced moment(s) of inertia of the pre-reactive complex extracted by *Eyringpy* from the *Gaussian* output file with the frequency and HR analysis.

Format: RED\_MOM\_INERT\_RC 89.2467 100.6895

- RED\_MOM\_INERT\_TS: Reduced moment(s) of inertia of the TS for the HR model.

Type: Float

Units: amu Bohr<sup>2</sup>

Default value: Reduced moment(s) of inertia of the TS extracted by *Eyringpy* from the *Gaussian* output file with the frequency and HR analysis.

Format: RED\_MOM\_INERT\_TS 89.2467 100.6895

- RED\_MOM\_INERT\_PC: Reduced moment(s) of inertia of the product complex for the HR model.

Type: Float

Units: amu Bohr<sup>2</sup>

Default value: Reduced moment of inertia(s) of the product complex extracted by *Eyringpy* from the *Gaussian* output file with the frequency and HR analysis.

Format: RED\_MOM\_INERT\_PC 89.2467 100.6895

- 
- RED\_MOM\_INERT\_Pn: Reduced moment(s) of inertia of the  $n$  product for the HR model.

Type: Float

Units: amu Bohr<sup>2</sup>

Default value: Reduced moment(s) of inertia of the  $n$  product extracted by *Eyringpy* from the *Gaussian* output file with the frequency and HR analysis.

Format: RED\_MOM\_INERT\_P1 89.2467 100.6895

- TORNSYM\_Rn: Torsional symmetry number(s) of the  $n$  reactant for the HR model.

Type: Integer

Default value: Torsional symmetry number(s) of the  $n$  reactant extracted by *Eyringpy* from the *Gaussian* output file with the frequency and HR analysis.

Format: TORNSYM\_R1 89.2467 100.6895

- TORNSYM\_RC: Torsional symmetry number(s) of the pre-reactive complex for the HR model.

Type: Integer

Default value: Torsional symmetry number(s) of the pre-reactive complex extracted by *Eyringpy* from the *Gaussian* output file with the frequency and HR analysis.

Format: TORNSYM\_RC 89.2467 100.6895

- TORNSYM\_TS: Torsional symmetry number(s) of the TS for the HR model.

---

Type: Float

Default value: Torsional symmetry number(s) of the TS extracted by *Eyringpy* from the *Gaussian* output file with the frequency and HR analysis.

Format: TORNSYM\_TS 89.2467 100.6895

- TORNSYM\_PC: Torsional symmetry number(s) of the product complex for the HR model.

Type: Integer

Default value: Torsional symmetry number(s) of the product complex extracted by *Eyringpy* from the *Gaussian* output file with the frequency and HR analysis.

Format: TORNSYM\_PC 89.2467 100.6895

- TORNSYM\_Pn: Torsional symmetry number(s) of the  $n$  product for the HR model.

Type: Integer

Default value: Torsional symmetry number(s) of the  $n$  product extracted by *Eyringpy* from the *Gaussian* output file with the frequency and HR analysis.

Format: TORNSYM\_P1 89.2467 100.6895

## Appendix C Supplementary Information of Chapter 2

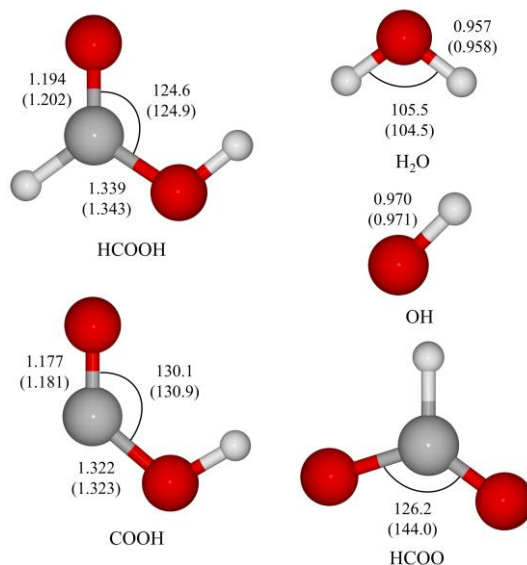


**Figure C1.** Geometries of the reactants and products of the hydrogen abstraction from formic acid by hydroxyl radical optimized at the M05-2X/6-311++G(d,p) level. Experimental values are between parenthesis. Bond lengths are in Angstrom and angles are in degrees.

**Table C1.** Recrossing factors (ratio  $k_{TST}/k_{VTST}$ ) of the gas phase hydrogen abstraction from formic acid by  $\cdot\text{OH}$  in the 298.15-440 K range.

T (K)	Ia	Ib	IIa	IIb	Overall
298.15	1.09	1.11	8.46	48.33	1.62
300.00	1.09	1.20	9.23	47.37	1.66
320.00	1.09	1.14	8.42	46.43	1.80



---

340.00	1.11	1.16	8.80	47.37	2.04
360.00	1.08	1.16	8.24	46.15	2.19
380.00	1.08	1.12	8.18	47.06	2.40
400.00	1.07	1.15	8.18	47.67	2.62
420.00	1.07	1.16	8.09	47.27	2.84
440.00	1.09	1.16	8.07	50.00	3.13

---

**Table C2.** Branching ratios, in percentage, of the gas phase hydrogen abstraction from formic acid by  $\cdot\text{OH}$  in the 298.15-440 K temperature range.

<b>T (K)</b>	<b><math>\Gamma_{Ia}</math></b>	<b><math>\Gamma_{Ib}</math></b>	<b><math>\Gamma_{IIa}</math></b>	<b><math>\Gamma_{IIb}</math></b>
<b>298.15</b>	<b>97.1</b>	<b>2.4</b>	<b>0.4</b>	<b>0.1</b>
300.00	97.1	2.5	0.4	0.1
320.00	85.2	14.0	0.7	0.1
340.00	84.3	14.5	1.1	0.2
360.00	82.5	15.6	1.7	0.2
380.00	81.1	16.2	2.3	0.4
400.00	78.3	17.9	3.2	0.5
420.00	76.4	18.8	4.2	0.6
440.00	75.1	19.1	5.0	0.8

---

---

## References

1. Eyring, H. *J. Chem. Phys.* **1935**, *3*, 107.
2. Daudel, R.; Lerroy, G.; Peeters, D.; Sana, M., *Quantum Chemistry*. John Wiley & Sons: Chichester, 1983.
3. Cheng, G.-J.; Zhang, X.; Chung, L. W.; Xu, L.; Wu, Y.-D. *J. Am. Chem. Soc.* **2015**, *137*, 1706.
4. Bao, J. L.; Truhlar, D. G. *Chem. Soc. Rev.* **2017**, *46*, 7548.
5. Truhlar, D. G.; Garrett, B. C. *Acc. Chem. Res.* **1980**, *13*, 440.
6. Truhlar, D. G.; Garrett, B. C. *Annu. Rev. Phys. Chem.* **1984**, *35*, 159.
7. Červinka, C.; Fulem, M.; Růžička, K. t. *J. Chem. Eng. Data* **2012**, *57*, 227.
8. Ayala, P. Y.; Schlegel, H. B. *J. Chem. Phys.* **1998**, *108*, 2314.
9. Červinka, C.; Fulem, M.; Růžička, K. t. *J. Chem. Eng. Data* **2013**, *58*, 1382.
10. Gao, Y.; He, T.; Li, X.; You, X. *Phys. Chem. Chem. Phys.* **2019**, *21*, 1928.
11. Dzib, E.; Merino, G. *WIREs Comput. Mol. Sci.* **2022**, *12*, e1583.
12. Alvarez-Idaboy, J. R.; Mora-Diez, N.; Boyd, R. J.; Vivier-Bunge, A. *J. Am. Chem. Soc.* **2001**, *123*, 2018.
13. Galano, A.; Alvarez-Idaboy, J. R.; Ruiz-Santoyo, M. E.; Vivier-Bunge, A. *J. Phys. Chem. A* **2002**, *106*, 9520.
14. Mora-Diez, N.; Alvarez-Idaboy, J. R.; Boyd, R. J. *J. Phys. Chem. A* **2001**, *105*, 9034.
15. Uc, V. H.; Alvarez-Idaboy, J. R.; Galano, A.; García-Cruz, I.; Vivier-Bunge, A. *J. Phys. Chem. A* **2006**, *110*, 10155.
16. Fernández-Ramos, A.; Ellingson, B. A.; Meana-Pañeda, R.; Marques, J. M.; Truhlar, D. G. *Theor. Chem. Acc.* **2007**, *118*, 813.

- 
17. Dzib Reyes, E. V. Eyringpy: Un Programa para calcular Propiedades Termoquímicas y Constantes de Velocidad de Reacciones en Fase Gaseosa y en Disolución. Cinvestav, Mérida, Yucatán, 2017.
  18. Wigner, E. *Phys. Rev.* **1932**, *40*, 749.
  19. Eckart, C. *Phys. Rev.* **1930**, *35*, 1303.
  20. Collins, F. C.; Kimball, G. E. *J. Colloid Sci.* **1949**, *4*, 425.
  21. Marcus, R. A. *J. Chem. Phys.* **1956**, *24*, 966.
  22. Marcus, R. A. *Rev. Mod. Phys.* **1993**, *65*, 599.
  23. Galano, A.; Alvarez-Idaboy, J. R. *J. Comput. Chem.* **2013**, *34*, 2430.
  24. Quintal, A.; Dzib, E.; Ortíz-Chi, F.; Jaque, P.; Restrepo, A.; Merino, G. *Int. J. Quantum Chem.* **2021**, *121*, e26684.
  25. Canneaux, S.; Bohr, F.; Henon, E. *J. Comput. Chem.* **2014**, *35*, 82.
  26. Duncan, W. T.; Bell, R. L.; Truong, T. N. *J. Comput. Chem.* **1998**, *19*, 1039.
  27. Arnaut, L. G.; Formosinho, S. J.; Burrows, H., *Chemical Kinetics: from Molecular Structure to Chemical Reactivity*, 1st ed.; Elsevier: The Netherlands, 2007.
  28. Klippenstein, S. J.; Pande, V. S.; Truhlar, D. G. *J. Am. Chem. Soc.* **2014**, *136*, 528.
  29. Vereecken, L.; Francisco, J. S. *Chem. Soc. Rev.* **2012**, *41*, 6259.
  30. Vereecken, L.; Glowacki, D. R.; Pilling, M. J. *Chem. Rev.* **2015**, *115*, 4063.
  31. Klippenstein, S. J. *Proc. Combust. Inst.* **2017**, *36*, 77.
  32. Elliott, S. N.; Moore III, K. B.; Copan, A. V.; Keçeli, M.; Cavallotti, C.; Georgievskii, Y.; Schaefer III, H. F.; Klippenstein, S. J. *Proc. Combust. Inst.* **2021**, *38*, 375.

- 
33. Miller, J. A.; Sivaramakrishnan, R.; Tao, Y.; Goldsmith, C. F.; Burke, M. P.; Jasper, A. W.; Hansen, N.; Labbe, N. J.; Glarborg, P.; Zádor, J. *Prog. Energy Combust. Sci.* **2021**, *83*, 100886.
34. Vazart, F.; Calderini, D.; Puzzarini, C.; Skouteris, D.; Barone, V. *J. Chem. Theory Comput.* **2016**, *12*, 5385.
35. Gamez-Garcia, V. G.; Galano, A. *J. Phys. Chem. A* **2017**, *121*, 7393.
36. Baiano, C.; Lupi, J.; Tasinato, N.; Puzzarini, C.; Barone, V. *Molecules* **2020**, *25*, 2873.
37. Cavallotti, C.; Pelucchi, M.; Georgievskii, Y.; Klippenstein, S. *J. Chem. Theory Comput.* **2018**, *15*, 1122.
38. Frisch, M. J.; Trucks, G. W.; Schlegel, H. B.; Scuseria, G. E.; Robb, M. A.; Cheeseman, J. R.; Scalmani, G.; Barone, V.; Petersson, G. A.; Nakatsuji, H.; Li, X.; Caricato, M.; Marenich, A. V.; Bloino, J.; Janesko, B. G.; Gomperts, R.; Mennucci, B.; Hratchian, H. P.; Ortiz, J. V.; Izmaylov, A. F.; Sonnenberg, J. L.; Williams-Young, D.; Ding, F.; Lipparini, F.; Egidi, F.; Goings, J.; Peng, B.; Petrone, A.; Henderson, T.; Ranasinghe, D.; Zakrzewski, V. G.; Gao, J.; Rega, N.; Zheng, G.; Chi-Hsiu, W. L.; Hada, M.; Ehara, M.; Toyota, K.; Fukuda, R.; Hasegawa, J.; Ishida, M.; Nakajima, T.; Honda, Y.; Kitao, O.; Nakai, H.; Vreven, T.; Throssell, K.; Montgomery, J., J. A.; Peralta, J. E.; Ogliaro, F.; Bearpark, M. J.; Heyd, J. J.; Brothers, E. N.; Kudin, K. N.; Staroverov, V. N.; Keith, T. A.; Kobayashi, R.; Normand, J.; Raghavachari, K.; Rendell, A. P.; Burant, J. C.; Iyengar, S. S.; Tomasi, J.; Cossi, M.; Millam, J. M.; Klene, M.; Adamo, C.; Cammi, R.; Ochterski, J. W.;
-

- 
- Martin, R. L.; Morokuma, K.; Farkas, O.; Foresman, J. B.; Fox, D. J. *Gaussian 16*, Revision B.01; Gaussian Inc.: Wallingford, CT, 2016.
39. Neese, F.; Wennmohs, F.; Becker, U.; Riplinger, C. *J. Chem. Phys.* **2020**, *152*, 224108.
40. Te Velde, G. t.; Bickelhaupt, F. M.; Baerends, E. J.; Fonseca Guerra, C.; van Gisbergen, S. J.; Snijders, J. G.; Ziegler, T. *J. Comput. Chem.* **2001**, *22*, 931.
41. Galano, A.; Alvarez-Idaboy, J. R.; Vivier-Bunge, A. *J. Chem. Educ.* **2006**, *83*, 481.
42. Galano, A.; Alvarez-Idaboy, J. R. *J. Comput. Chem.* **2014**, *35*, 2019.
43. Sun, Y.; Somers, K. P.; Wang, Q.-D.; Farrell, C.; Curran, H. J. *Phys. Chem. Chem. Phys.* **2020**, *22*, 27241.
44. Evans, M. G.; Polanyi, M. *Trans. Faraday Soc.* **1935**, *31*, 875.
45. Marcus, R. A. *J. Chem. Phys.* **1952**, *20*, 359.
46. Henriksen, N. E.; Hansen, F. Y., *Theories of Molecular Reaction Dynamics: the Microscopic foundation of Chemical Kinetics*, 1st ed.; Oxford University Press: The USA, 2008.
47. Jensen, F., *Introduction to Computational Chemistry*, 2nd ed.; Wiley: The UK, 2006.
48. Fernández-Ramos, A.; Miller, J. A.; Klippenstein, S. J.; Truhlar, D. G. *Chem. Rev.* **2006**, *106*, 4518.
49. Dzib, E.; Cabellos, J. L.; Ortíz-Chi, F.; Pan, S.; Galano, A.; Merino, G. *Int. J. Quantum Chem.* **2019**, *119*, e25686.
50. Galano, A. *J. Mex. Chem. Soc.* **2015**, *59*, 231.
-

- 
51. Klippenstein, S. J.; Cavallotti, C., Ab initio kinetics for pyrolysis and combustion systems. In *Computer Aided Chemical Engineering*, Elsevier: 2019; Vol. 45, pp 115.
  52. Isaacson, A. D.; Truhlar, D. G. *J. Chem. Phys.* **1982**, *76*, 1380.
  53. Isaacson, A. D.; Truhlar, D. G.; Rai, S. N.; Steckler, R.; Hancock, G. C.; Garrett, B. C.; Redmon, M. J. *Comput. Phys. Commun.* **1987**, *47*, 91.
  54. Lu, D.-h.; Truong, T. N.; Melissas, V. S.; Lynch, G. C.; Liu, Y.-P.; Garrett, B. C.; Steckler, R.; Isaacson, A. D.; Rai, S. N.; Hancock, G. C.; Lauderdale, J. G.; Joseph, T.; Truhlar, D. G. *Comput. Phys. Commun.* **1992**, *71*, 235.
  55. Steckler, R.; Hu, W.-P.; Liu, Y.-P.; Lynch, G. C.; Garrett, B. C.; Isaacson, A. D.; Melissas, V. S.; Lu, D.-h.; Truong, T. N.; Rai, S. N.; Hancock, G. C.; Lauderdale, J. G.; Joseph, T.; Truhlar, D. G. *Comput. Phys. Commun.* **1995**, *88*, 341.
  56. Barker, J. R. *Int. J. Chem. Kinet.* **2001**, *33*, 232.
  57. Smedarchina, Z.; Fernández-Ramos, A.; Siebrand, W. *J. Comput. Chem.* **2001**, *22*, 787.
  58. Barreto, P. R. P.; Vilela, A. F. A.; Gargano, R. *J. Mol. Struct.: THEOCHEM* **2003**, *639*, 167.
  59. Barreto, P. R. P.; Vilela, A. F. A.; Gargano, R. *Int. J. Quantum Chem.* **2005**, *103*, 685.
  60. Euclides, H. O.; Barreto, P. R. P. *J. Mol. Model.* **2017**, *23*, 176.
  61. Pfaendtner, J.; Yu, X.; Broadbelt, L. J. *Theor. Chem. Acc.* **2007**, *118*, 881.
  62. Ghysels, A.; Verstraelen, T.; Hemelsoet, K.; Waroquier, M.; Van Speybroeck, V. *J. Chem. Inf. Model.* **2010**, *50*, 1736.
  63. Glowacki, D. R.; Liang, C.-H.; Morley, C.; Pilling, M. J.; Robertson, S. H. *J. Phys. Chem. A* **2012**, *116*, 9545.
-

- 
64. Zheng, J.; Mielke, S. L.; Clarkson, K. L.; Truhlar, D. G. *Comput. Phys. Commun.* **2012**, *183*, 1803.
65. Zheng, J.; Meana-Pañeda, R.; Truhlar, D. G. *Comput. Phys. Commun.* **2013**, *184*, 2032.
66. Duong, M. V.; Nguyen, H. T.; Truong, N.; Le, T. N. M.; Huynh, L. K. *Int. J. Chem. Kinet.* **2015**, *47*, 564.
67. Le, T. H.; Do, S. T.; Huynh, L. K. *Comput. Theor. Chem.* **2017**, *1100*, 61.
68. Le, T. H.; Tran, T. T.; Huynh, L. K. *Chemom. Intell. Lab. Syst.* **2018**, *172*, 10.
69. Gao, C. W.; Allen, J. W.; Green, W. H.; West, R. H. *Comput. Phys. Commun.* **2016**, *203*, 212.
70. Hjorth Larsen, A.; Jørgen Mortensen, J.; Blomqvist, J.; Castelli, I. E.; Christensen, R.; Dułak, M.; Friis, J.; Groves, M. N.; Hammer, B.; Hargus, C.; Hermes, E. D.; Jennings, P. C.; Bjerre Jensen, P.; Kermode, J.; Kitchin, J. R.; Leonhard Kolsbjerg, E.; Kubal, J.; Kaasbjerg, K.; Lysgaard, S.; Bergmann Maronsson, J.; Maxson, T.; Olsen, T.; Pastewka, L.; Peterson, A.; Rostgaard, C.; Schiøtz, J.; Schütt, O.; Strange, M.; Thygesen, K. S.; Vegge, T.; Vilhelmsen, L.; Walter, M.; Zeng, Z.; Jacobsen, K. *W. J. Phys.: Condens. Matter* **2017**, *29*, 273002.
71. Ferro-Costas, D.; Cordeiro, M. N. D.; Truhlar, D. G.; Fernández-Ramos, A. *Comput. Phys. Commun.* **2018**, *232*, 190.
72. Machado, H. G.; Sanches-Neto, F. O.; Coutinho, N. D.; Mundim, K. C.; Palazzetti, F.; Carvalho-Silva, V. H. *Molecules* **2019**, *24*, 3478.
73. Ferro-Costas, D.; Truhlar, D. G.; Fernández-Ramos, A. *Comput. Phys. Commun.* **2020**, *256*, 107457.
-

- 
74. Garrett, B. C.; Truhlar, D. G., Variational transition state theory. In *Theory and Applications of Computational Chemistry*, Elsevier: 2005; pp 67.
75. Fernandez-Ramos, A.; Ellingson, B. A.; Garrett, B. C.; Truhlar, D. G., Variational transition state theory with multidimensional tunneling. In *Reviews in Computational Chemistry*, Lipkowitz, K. B.; Cundari, T. R., Eds. John Wiley & Sons: 2007; Vol. 23, pp 125.
76. Bucko, T.; Hafner, J. *J. Phys.: Condens. Matter* **2010**, *22*, 384201.
77. Chen, X.; Goldsmith, C. F. *J. Phys. Chem. A* **2020**, *124*, 1038.
78. Zavala-Oseguera, C.; Alvarez-Idaboy, J. R.; Merino, G.; Galano, A. *J. Phys. Chem. A* **2009**, *113*, 13913.
79. Ebert, L., In *Leipziger Vorträge*, 1929; p 74.
80. Moss, G. *Pure Appl. Chem.* **1996**, *68*, 2193.
81. Ellingson, B. A.; Lynch, V. A.; Mielke, S. L.; Truhlar, D. G. *J. Chem. Phys.* **2006**, *125*, 084305.
82. Zheng, J.; Yu, T.; Papajak, E.; Alecu, I.; Mielke, S. L.; Truhlar, D. G. *Phys. Chem. Chem. Phys.* **2011**, *13*, 10885.
83. Schmalz, F.; Kopp, W. A.; Kröger, L. C.; Leonhard, K. *ACS Omega* **2020**, *5*, 2242.
84. Pitzer, K. S.; Gwinn, W. D. *J. Chem. Phys.* **1942**, *10*, 428.
85. Pitzer, K. S. *J. Chem. Phys.* **1946**, *14*, 239.
86. Ochterski, J. W. Thermochemistry in Gaussian 2000. <http://gaussian.com/>.
87. Cramer, C. J., *Essentials of Computational Chemistry: Theories and Models*, 2nd ed.; Wiley: The UK, 2004.
-



- 
88. Foresman, J. B.; Frisch, Æ., *Exploring Chemistry with Electronic Structure Methods*, 3rd ed.; Gaussian, Inc.: Wallingford, CT, 2015.
  89. McQuarrie, D. A., *Statistical Mechanics*, Harper & Row: The USA, 1973.
  90. Reinisch, G.; Leyssale, J.-M.; Vignoles, G. L. *J. Chem. Phys.* **2010**, *133*, 154112.
  91. Janakiraman, D.; Sebastian, K. *Comput. Theor. Chem.* **2012**, *988*, 6.
  92. Arfken, G. B.; Weber, H. J., *Mathematical Methods for Physicists*. 6 ed.; Elsevier: The USA, 2005.
  93. Gadella, M.; Giacomini, H.; Lara, L. *Appl. Math. Comput.* **2015**, *271*, 436.
  94. McClurg, R. B.; Flagan, R. C.; Goddard III, W. A. *J. Chem. Phys.* **1997**, *106*, 6675.
  95. Truhlar, D. G. *J. Comput. Chem.* **1991**, *12*, 266.
  96. McQuarrie, D. A.; Simon, J. D., *Molecular Thermodynamics*, University Science Books: 1999.
  97. Dzib, E.; Quintal, A.; Ortíz-Chi, F.; Merino, G. *Eyringpy*, 3.0; Cinvestav: Mérida, Yucatán, 2022.
  98. Pollak, E.; Pechukas, P. *J. Am. Chem. Soc.* **1978**, *100*, 2984.
  99. Minkin, V. I. *Pure Appl. Chem.* **1999**, *71*, 1919.
  100. González-Lafont, À.; Lluch, J. M. *J. Mol. Struct.: THEOCHEM* **2004**, *709*, 35.
  101. Frisch, M. J.; Trucks, G. W.; Schlegel, H. B.; Scuseria, G. E.; Robb, M. A.; Cheeseman, J. R.; Scalmani, G.; Barone, V.; Petersson, G. A.; Nakatsuji, H.; Li, X.; Caricato, M.; Marenich, A. V.; Bloino, J.; Janesko, B. G.; Gomperts, R.; Mennucci, B.; Hratchian, H. P.; Ortiz, J. V.; Izmaylov, A. F.; Sonnenberg, J. L.; Williams-Young, D.; Ding, F.; Lipparini, F.; Egidi, F.; Goings, J.; Peng, B.; Petrone, A.; Henderson, T.; Ranasinghe, D.; Zakrzewski, V. G.; Gao, J.; Rega, N.; Zheng, G.;

- 
- Liang, W.; Hada, M.; Ehara, M.; Toyota, K.; Fukuda, R.; Hasegawa, J.; Ishida, M.; Nakajima, T.; Honda, Y.; Kitao, O.; Nakai, H.; Vreven, T.; Throssell, K.; Montgomery, J. A., Jr.; Peralta, J. E.; Ogliaro, F.; Bearpark, M.; Heyd, J. J.; Brothers, E.; Kudin, K. N.; Staroverov, V. N.; Keith, T.; Kobayashi, R.; Normand, J.; Raghavachari, K.; Rendell, A.; Burant, J. C.; Iyengar, S. S.; Tomasi, J.; Cossi, M.; Millam, J. M.; Klene, M.; Adamo, C.; Cammi, R.; Ochterski, J. W.; Martin, R. L.; Morokuma, K.; Farkas, O.; Foresman, J. B.; Fox, D. J. *Gaussian 09*, Revision A. 02; Gaussian Inc.: Wallingford, CT, 2009.
102. Frisch, M. J.; Trucks, G. W.; Schlegel, H. B.; Scuseria, G. E.; Robb, M. A.; Cheeseman, J. R.; Scalmani, G.; Barone, V.; Mennucci, B.; Petersson, G. A.; Nakatsuji, H.; Caricato, M.; Li, X.; Hratchian, H. P.; Izmaylov, A. F.; Bloino, J.; Zheng, G.; Sonnenberg, J. L.; Hada, M.; Ehara, M.; Toyota, K.; Fukuda, R.; Hasegawa, J.; Ishida, M.; Nakajima, T.; Honda, Y.; Kitao, O.; Nakai, H.; Vreven, T.; Montgomery, J., J. A. ; Peralta, J. E.; Ogliaro, F.; Bearpark, M.; Heyd, J. J.; Brothers, E.; Kudin, K. N.; Staroverov, V. N.; Keith, T.; Kobayashi, R.; Normand, J.; Raghavachari, K.; Rendell, A.; Burant, J. C.; Iyengar, S. S.; Tomasi, J.; Cossi, M.; Rega, N.; Millam, J. M.; Klene, M.; Knox, J. E.; Cross, J. B.; Bakken, V.; Adamo, C.; Jaramillo, J.; Gomperts, R.; Stratmann, R. E.; Yazyev, O.; Austin, A. J.; Cammi, R.; Pomelli, C.; Ochterski, J. W.; Martin, R. L.; Morokuma, K.; Zakrzewski, V. G.; Voth, G. A.; Salvador, P.; Dannenberg, J. J.; Dapprich, S.; Daniels, A. D.; Farkas, O.; Foresman, J. B.; Ortiz, J. V.; Cioslowski, J.; Fox, D. J. *Gaussian 09*, Revision D.01; Gaussian Inc.: Wallingford, CT, 2013.
-

- 
103. Lemmon, E. W., Thermophysical properties of fluids. National Institute of Standards and Technology: 2009.
104. Fukui, K. *J. Phys. Chem.* **1970**, *74*, 4161.
105. Fukui, K. *Acc. Chem. Res.* **1981**, *14*, 363.
106. Zavala-Oseguera, C.; Galano, A. *J. Chem. Theory Comput.* **2009**, *5*, 1295.
107. Toro-Labbé, A. *J. Phys. Chem. A* **1999**, *103*, 4398.
108. Zhao, Y.; Schultz, N. E.; Truhlar, D. G. *J. Chem. Theory Comput.* **2006**, *2*, 364.
109. Vega-Rodriguez, A.; Alvarez-Idaboy, J. R. *Phys. Chem. Chem. Phys.* **2009**, *11*, 7649.
110. Galano, A.; Alvarez-Idaboy, J. R. *Org. Lett.* **2009**, *11*, 5114.
111. Black, G.; Simmie, J. M. *J. Comput. Chem.* **2010**, *31*, 1236.
112. Furuncuoglu, T.; Ugur, I.; Degirmenci, I.; Aviyente, V. *Macromolecules* **2010**, *43*, 1823.
113. Gao, T.; Andino, J. M.; Alvarez-Idaboy, J. R. *Phys. Chem. Chem. Phys.* **2010**, *12*, 9830.
114. Galano, A.; Macías-Ruvalcaba, N. A.; Medina Campos, O. N.; Pedraza-Chaverri, J. *J. Phys. Chem. B* **2010**, *114*, 6625.
115. Anglada, J. M. *J. Am. Chem. Soc.* **2004**, *126*, 9809.
116. Herzberg, G., *Molecular Spectra and Molecular Structure: III. Electronic Spectra and Electronic Structure of Polyatomic Molecules*, Von Nostrand Reinhold Co.: The USA, 1966.
117. Huber, K. P.; Herzberg, G., *Molecular Spectra and Molecular Structure: IV. Constants of Diatomic Molecules*, Springer: The USA, 1979.
-

- 
118. Kim, E.; Bradforth, S.; Arnold, D.; Metz, R.; Neumark, D. *J. Chem. Phys.* **1995**, *103*, 7801.
119. Iuga, C.; Alvarez-Idaboy, J. R.; Vivier-Bunge, A. *J. Phys. Chem. A* **2011**, *115*, 5138.
120. Zetzsch, C.; Stuhl, F. In *Rate constants for reactions of OH with carbonic acids*, Physico-Chemical Behaviour of Atmospheric Pollutants, Netherlands, Netherlands, 1982; pp 129.
121. Wine, P.; Astalos, R.; Mauldin III, R. *J. Phys. Chem.* **1985**, *89*, 2620.
122. Jolly, G. S.; McKenney, D. J.; Singleton, D. L.; Paraskevopoulos, G.; Bossard, A. R. *J. Phys. Chem.* **1986**, *90*, 6557.
123. Singleton, D. L.; Paraskevopoulos, G.; Irwin, R. S.; Jolly, G. S.; McKenney, D. J. *J. Am. Chem. Soc.* **1988**, *110*, 7786.
124. Manion, J.; Huie, R.; Levin, R.; Burgess, D. J.; Orkin, V.; Tsang, W.; McGivern, W.; Hudgens, J.; Knyazev, V.; Atkinson, D.; Chai, E.; Tereza, A.; Lin, C.-Y.; Allison, T.; Mallard, W.; Westley, F.; Herron, J.; Hampson, R.; Frizzell, D., NIST Chemical Kinetics Database. National Institute of Standards and Technology: Gaithersburg, Maryland, 2015.
125. Bravo-Pérez, G.; Alvarez-Idaboy, J. R.; Jiménez, A. G.; Cruz-Torres, A. *Chem. Phys.* **2005**, *310*, 213.
126. Bonard, A.; Daële, V.; Delfau, J.-L.; Vovelle, C. *J. Phys. Chem. A* **2002**, *106*, 4384.